Follicular helper T cell profiles predict response to costimulation blockade in type 1 diabetes

Natalie M. Edner[1,5], Frank Heuts[1,5], Niclas Thomas[1], Chun Jing Wang[1], Lina Petersone[1], Rupert Kenefeck[1], Alexandros Kogimtzis[1], Vitalijs Ovcinnikovs[1], Ellen M. Ross[1], Elisavet Ntavli[1], Yassin Elfaki[1], Martin Eichmann[2], Roman Baptista[2], Philip Ambery[3], Lutz Jermutus[4], Mark Peakman[2], Miranda Rosenthal[1] and Lucy S.K. Walker[1]

[1]Institute of Immunity & Transplantation, University College London Division of Infection & Immunity, Royal Free Campus, London, NW3 2PF, United Kingdom. [2]Department of Immunobiology, King's College London, London SE1 9RT, United Kingdom. [3]Late-stage Development, Cardiovascular, Renal and Metabolism (CVRM), BioPharmaceuticals R&D, AstraZeneca, Gothenburg, Sweden. [4]Research and Early Development, Cardiovascular, Renal and Metabolism (CVRM), BioPharmaceuticals R&D, AstraZeneca, Cambridge, United Kingdom.

[5]These authors contributed equally to this work.

Corresponding author: Prof Lucy S.K. Walker, Institute of Immunity & Transplantation, University College London Division of Infection & Immunity, Royal Free Campus, London, UK NW3 2PF. Tel: [+]44 (0)20 7794 0500 ext 22468. Email: lucy.walker@ucl.ac.uk

Abstract

Follicular helper T cells (Tfh) are implicated in type 1 diabetes (T1D) and their development has been linked to CD28 costimulation. We tested whether Tfh were decreased by costimulation blockade using the CTLA-4-Ig fusion protein (Abatacept) in a mouse model of diabetes and in individuals with new onset T1D. Unbiased bioinformatic analysis identified that ICOS$^+$ Tfh, and other ICOS$^+$ populations including T-peripheral helper cells, were highly sensitive to costimulation blockade. We were able to use pre-treatment Tfh profiles to derive a model that could predict clinical response to Abatacept in individuals with T1D. Using two independent approaches we demonstrated that higher frequencies of ICOS$^+$ Tfh at baseline were associated with a poor clinical response following Abatacept administration. Tfh analysis may therefore represent a new stratification tool, permitting the identification of individuals most likely to benefit from costimulation blockade.

CD28 costimulation licenses T cells for effective activation and is a key therapeutic target in autoimmunity. The natural regulator of CD28 is the inhibitory receptor CTLA-4, and a soluble version of this molecule has been developed for therapeutic use. Soluble CTLA-4 (a fusion protein with human immunoglobulin; CTLA-4-Ig) is widely used in autoimmune conditions including rheumatoid arthritis (RA), psoriatic arthritis and juvenile idiopathic arthritis[1, 2, 3]. Studies in the NOD mouse model of type 1 diabetes (T1D) suggested a protective effect of CTLA-4-Ig in this disease setting[4] leading to a trial of the clinically licensed CTLA-4-Ig molecule Abatacept (Orencia®; Bristol-Myers Squibb) in individuals with new onset T1D. A randomised double-blind placebo-controlled trial showed that adjusted C-peptide levels were 59% higher in recipients of Abatacept at 2 years compared with placebo[5], and the beneficial effects were largely maintained a year following therapy cessation[6], although it was clear that some individuals benefited more than others. Thus, CTLA-4-Ig-based costimulation blockade in both mice and humans implicates the CD28 pathway in T1D pathogenesis, however the precise CD28-dependent processes involved remain ill-defined. Identifying and monitoring these could potentially help explain, and even predict, why certain individuals make a better response to costimulation blockade than others.

Although T1D has classically been considered to be a T_H1-mediated pathology, a signature of follicular helper T cell (Tfh) differentiation was identified in this disease setting[7]. Tfh support B cell responses within the germinal centers (GC) of secondary lymphoid tissues and are characterised by markers such as CXCR5, ICOS and PD-1 as well as the transcription factor Bcl6[8, 9, 10]. Memory Tfh in the blood share T cell receptor (TCR) clonotypes with their lymphoid tissue counterparts[11, 12] and can home to GC in response to secondary immunisation[13, 14]. Murine T cells responding to a pancreatic self-antigen adopted a Tfh phenotype and GC were formed in the pancreatic lymph nodes (PanLN) of mice developing diabetes[7]. Likewise, in humans with T1D a higher proportion of blood-borne Tfh were observed within the memory compartment than in matched non-diabetic individuals[7], and similar data were obtained in two independent T1D patient cohorts[15, 16].

Subsequent studies showed that circulating cells with a Tfh phenotype were increased in children with multiple islet autoantibodies at risk of developing T1D[17, 18]. Thus, circulating Tfh-like cells have been associated with T1D in multiple patient cohorts, and increases in these cells may precede the development of overt disease.

CD28 has long been implicated in the development of Tfh and the provision of T cell help for antibody responses. Mice deficient in the CD28 ligands, CD80 and CD86, fail to form GC[19], associated with an inability of their T cells to upregulate the chemokine receptor CXCR5 that guides T cells towards B cell follicles[20]. More recently, it was reported that Tfh differentiation was sensitive to the strength of CD28 engagement, and that this could be modulated by CTLA-4[21]. A clear prediction of these studies is that use of CTLA4-Ig (Abatacept) to inhibit CD28 costimulation would be expected to decrease Tfh differentiation, and there are already suggestions that this may be the case in primary Sjogren's syndrome[22], rheumatoid arthritis[23] and multiple sclerosis[24]. We were therefore interested to assess the impact of Abatacept on Tfh populations in T1D.

Here we show that Tfh are a sensitive biomarker of costimulation blockade in both mice and humans with T1D and reveal that pre-treatment Tfh profiles can be used to predict response to Abatacept. These data ascribe new value to Tfh analysis and suggest its potential as a stratification tool prior to immunotherapy.

Results

Abatacept decreases immunisation-induced Tfh in mice

Costimulation blockade using antibodies against CD80 and CD86 decreased the capacity of adoptively transferred TCR transgenic T cells to differentiate into Tfh following immunisation[21]. We predicted that costimulation blockade with Abatacept would yield similar results, since this reagent binds to CD80 and CD86 in a manner that inhibits their engagement of CD28. We sought to confirm this, and concurrently to probe the kinetic requirements for effective Tfh inhibition, by providing Abatacept at different timepoints (**Fig. 1a**). We reasoned that the timing of costimulation blockade was an important consideration given that in autoimmune settings, treatment is likely to be delivered when the T cell response is already underway. Initiation of Abatacept treatment one day prior to immunisation (d-1) with ovalbumin (OVA) resulted in DO11.10 T cells exhibiting a significantly lower frequency (**Fig. 1b,c**) and absolute number (**Fig. 1d**) of Tfh than in Control-Ig treated animals. This was associated with inhibition of GC B cell formation as well as a decrease in expression of molecules involved in T cell / B cell collaboration such as CD40L and ICOS (**Fig. 1b-d**). Delaying costimulation blockade until 2 days after immunisation partially reduced its capacity to inhibit Tfh, and delaying it until day 4 abrogated the effects on Tfh and GC B cells (**Fig. 1**). Thus, costimulation blockade with Abatacept reduced Tfh, but delaying its administration rendered it less effective.

Abatacept decreases Tfh in a mouse model of diabetes

The inability of Abatacept to inhibit Tfh when delivered 4 days after immunisation raised the possibility that T cells already engaged in a response to autoantigen may be resistant to the Tfh modulating effects of this drug. To explore this idea, we examined the same TCR transgenic T cells responding to a pancreas-expressed, rather than immunised, protein. Mice that express the DO11.10 TCR transgene in conjunction with its cognate antigen in pancreatic beta cells (DO11.10 x RIP-mOVA mice) develop spontaneous islet autoimmunity and diabetes with 100% penetrance[25]. In

these mice, islet-expressed OVA is presented to T cells in the PanLN[26], and this is associated with T cell differentiation to a Tfh phenotype[7]. All mice manifest autoimmune islet infiltration by 5 weeks of age and we have established that CD28 costimulation is required for diabetes development (data not shown). To assess the impact of costimulation blockade on Tfh cells in the setting of an ongoing immune response to pancreatic autoantigen, we administered a short course of Abatacept to DO11.10 x RIP-mOVA mice (**Fig. 2a**). The results of this experiment revealed a decrease in Tfh at the site of antigen presentation (PanLN) as well as the spleen (**Fig. 2b,c**). Thus, even though T cell priming and Tfh differentiation were already underway prior to treatment, Abatacept was able to suppress the Tfh response.

Abatacept decreases circulating Tfh in type 1 diabetes patients

To assess whether Abatacept decreased circulating Tfh in humans with T1D, we obtained access to frozen samples from individuals with new onset T1D treated with Abatacept or placebo *via* Trialnet Study TN09 (NCT00505375). We were provided with samples from 36 Abatacept-treated individuals and 14 placebo-treated individuals, with 3 samples typically being available for each individual: baseline, and 1 and 2 years post treatment. Associated clinical data revealed a relative preservation of C-peptide in Abatacept-treated individuals compared with placebo-treated individuals (**Supplementary Fig. 1**), in line with the original trial results from the entire cohort[5]. Samples were stained with a panel of T cell markers including ones associated with a Tfh phenotype (for gating strategy see **Supplementary Fig. 2**). Since we previously showed that circulating $CD4^+CD45RA^-CXCR5^+$ cells (Tfh) were overrepresented in humans with T1D[7], we first examined whether this population was Abatacept-sensitive. Our analysis revealed that Tfh were significantly decreased after Abatacept treatment at both 1 and 2 year timepoints, whereas this was not the case in the placebo-treated control group (**Fig. 3a**). Principal component analysis of gated flow cytometry data revealed that the highest proportion of variance in this dataset is explained by Abatacept-induced changes, since treated samples are separated from untreated

150 samples along PC1 for Abatacept treatment but not placebo treatment (**Fig. 3b**). The major cell
151 population contributing to this separation was T cells expressing CXCR5 and ICOS (**Fig. 3c**).
152 $CCR7^{lo}PD\text{-}1^{+}CXCR5^{+}$ cells, previously identified as circulating Tfh precursors that correlate with
153 disease activity in autoimmunity[27], also contributed to PC1 and were decreased by Abatacept
154 treatment (here called $CCR7^{-}PD\text{-}1^{+}$ Tfh) (**Fig. 3c**). Graphed datapoints for the $ICOS^{+}PD\text{-}1^{+}$ Tfh
155 and $CCR7^{-}PD\text{-}1^{+}$ Tfh populations are provided for illustrative purposes, and depict the Abatacept-
156 induced change in cell frequency (**Fig. 3d**). To study the impact on Tfh subsets, additional trial
157 samples were analysed with a panel incorporating the chemokine receptors CXCR3 and CCR6[28].
158 The Abatacept-induced reduction of Tfh, and particularly $ICOS^{+}PD\text{-}1^{+}$Tfh, was corroborated,
159 however there was no obvious skewing of the Tfh subpopulations defined by CXCR3 and/or CCR6
160 expression (**Supplementary Fig. 3**). Overall, these findings demonstrated that cells expressing Tfh
161 markers were amongst the populations most affected by costimulation blockade.
162
163 **Additional Abatacept-sensitive populations in type 1 diabetes revealed by CellCnn**
164 Given the bias associated with manual gating, we tested whether unbiased analysis would also
165 identify a change in Tfh-like cells following Abatacept treatment. We used the machine-learning
166 algorithm CellCnn[29], a representation learning approach using convolutional neural networks
167 designed to identify rare cell subsets associated with disease status in a data-driven way. When
168 samples are split into 2 groups (e.g. Abatacept versus placebo), this approach is able to establish
169 marker expression profiles (termed filters) of individual cells whose frequency is associated with
170 the assigned group. In our analysis, CellCnn identified a filter whose corresponding cells were
171 present at high frequencies in all samples at baseline and in placebo treated samples, but were
172 significantly reduced in Abatacept-treated samples after two years of treatment (**Fig. 4a**), indicating
173 that this particular filter was associated with Abatacept-induced changes. Since filters detected by
174 CellCnn do not necessarily represent a homogenous cell population, k-means clustering was applied
175 to identify individual cell types affected by Abatacept treatment. In total, 6 clusters were found

(**Fig. 4b**) that showed distinct expression profiles of the selected markers. By overlaying these cell clusters on flow cytometry data (**Fig. 4c, Supplementary Fig. 4**) we ascribed names to them that we believe reflect their identity, and assessed the change in the frequency of these populations in Abatacept or placebo treated individuals (**Fig. 4d**). Consistent with our original manual gating approach, CellCnn identified both $ICOS^{+}PD\text{-}1^{+}$ Tfh (cluster 1) and $ICOS^{+}PD\text{-}1^{-}$ Tfh (cluster 2) to be decreased by Abatacept. A third cluster, comprising memory cells that lack CXCR5 but co-express ICOS and PD-1 (cluster 3), was also identified as Abatacept responsive **(Fig. 4d**). This phenotype is reminiscent of T-peripheral helper cells (Tph) that were identified in the rheumatoid joint and are increased in individuals with higher disease activity[30]. Manual gating of Tph confirmed a significant reduction in this population in people receiving Abatacept but not placebo at both year 1 and year 2 (**Fig. 4e**). CellCnn also identified Treg (cluster 4) to be Abatacept-sensitive, consistent with published literature[31, 32], in addition to two other clusters characterised by ICOS expression ($ICOS^{+}$ memory; cluster 5, $ICOS^{+}$ naive; cluster 6). Note that the term "naive" is used as shorthand to reflect the fact that the cells in cluster 6 are $CD45RA^{+}$, however their CD45RA expression level is slightly lower than bona fide naive T cells (**Fig. 4c**, cluster 6), suggesting they are antigen experienced. Thus machine-learning identified 2 Tfh populations and 4 additional populations to be Abatacept-sensitive, all of which expressed ICOS.

Since Tph have not previously been reported to be costimulation dependent, and $ICOS^{+}$ naive cells have not previously been described, we explored these populations further in our mouse model of diabetes. Cells with a "Tph" or "$ICOS^{+}$ naive" phenotype could be identified in mice (**Fig. 5a,d**), were enriched in autoimmune animals (**Fig. 5b,e**), and were reduced following Abatacept treatment (**Fig. 5c,f**). These murine data provide additional support for the costimulation sensitivity of these 2 populations.

To further explore the identity of the "Tph" population identified by CellCnn, additional trial samples were analysed. "Tph" cells were also decreased by Abatacept in this set of samples, and their expression of markers such as CCR5, CCR2, HLA-DR and CD38 was similar to that of Tph

identified by standard gating ($CXCR5^{-}PD\text{-}1^{hi}$)[30] (**Fig. 6a-c**). Applying CellCnn to these data identified a cluster of cells expressing Tph markers to be costimulation-sensitive (**Fig. 6d,e**). Overall, machine learning approaches indicated that populations with the characteristics of Tfh and Tph, as well as additional $ICOS^{+}$ populations, were strongly reduced after Abatacept treatment.

Baseline Tfh phenotype is associated with clinical response to Abatacept

We next explored whether an individual's clinical response following Abatacept treatment could be predicted from their T cell phenotype at baseline. Clinical response was assessed by relative C-peptide retention at the 2-year timepoint. Gated flow cytometry data were used, with a Tph gate and an $ICOS^{+}$ naive gate being added on the basis of their identification in the above analysis (**Supplementary Fig. 5a**). Age at diagnosis was also included since there is evidence that diagnosis at a young age is associated with a more rapid loss of beta cells[33]. Within the Abatacept-treated subjects, the 10 with the best clinical response (responders) and the 10 with the poorest response (non-responders) (**Fig. 7a**) were used to build a predictive model using gradient boosting[34, 35]. Pairwise correlation comparisons were conducted between features to identify and remove features that were highly correlated (Pearson correlation coefficient greater than 0.95), ensuring feature importance could be legitimately interpreted from our gradient boosting model (**Supplementary Fig. 5b**): where two features were shown to be highly correlated, the one least correlated with outcome was removed from the set of features used to build the predictive model. The gradient boosting model was constructed using nested leave-one-out cross validation. Each of the *n* patients was iteratively removed from the dataset and kept aside for testing purposes. The remaining *n-1* baseline samples were used for model training and hyperparameter (learning rate, maximum depth and number of estimators) tuning using 3-fold cross validation. The optimal model from this training process was then used to make a prediction on the "left-out" sample, and feature weights were recorded.

We were able to predict response to Abatacept with 85% accuracy and an area under curve (AUC) of 0.81 (**Fig. 7b**). The two features that emerged as being most important in predicting C-peptide retention following Abatacept treatment were $ICOS^+$ Tfh ($CD3^+CD4^+CD45RA^-CXCR5^+ICOS^+$) and $CXCR5^+$ naive cells ($CD3^+CD4^+CXCR5^+CD45RA^+$) **(Fig. 7c,d)**. Again, the term "naive" is used as shorthand for $CD45RA^+$, however cells in this gate have lower expression of CD45RA than naive T cells (see "$CXCR5^+$ naive" quadrant in **Supplementary Fig. 2**). $ICOS^-PD\text{-}1^-$ Tfh also contribute to predictive power in this model, with opposing directionality to $ICOS^+$ Tfh as expected (**Fig. 7d**). The $CCR7^{lo}PD\text{-}1^+CXCR5^+$ cells shown previously[27] to correlate with an active Tfh program were also identified in the model ($CCR7^-PD\text{-}1^+$ Tfh) **(Fig. 7c,d)**. Grouped time-series plots illustrate the dynamic change in the frequencies of these cell populations over time (**Supplementary Fig. 5c**) illustrating that responder and non-responder populations are broadly non-overlapping both before and during Abatacept treatment. Note that only baseline data were used to generate the model, avoiding the caveat that Abatacept treatment directly alters the frequencies of some of these populations.

As an independent approach, we were interested in whether data-driven analysis would detect similar cell subsets at baseline that differed between individuals who went on to make good or poor clinical responses following Abatacept therapy. Using CellCnn we were able to identify two filters, one of which shows higher frequencies of corresponding cells in samples from the 10 individuals exhibiting the poorest clinical response, while the other exhibits an inverse relationship, leading us to label these filters as "Non-Responder" and "Responder", respectively (**Fig. 8a,b**). In the non-responder filter, k-means clustering revealed 3 statistically significant T cell clusters; $ICOS^+PD\text{-}1^{hi}$Tfh, $ICOS^{int}PD\text{-}1^{lo}$Tfh and $ICOS^{hi}PD\text{-}1^{lo}CXCR5^-$ T cells (**Fig. 8c, Supplementary Fig. 6a,b**). The first 2 of these provide independent support for the predictive power of the $ICOS^+$ Tfh population identified in our gradient boosting model. Indeed, cells identified by CellCnn in those clusters overlaid the manual gates used for the predictive model (**Supplementary Fig. 7a)**.

ICOS^{+}PD-1^{hi} Tfh partially encompasses the CCR7^{-}PD-1^{+} Tfh population also identified by the model (**Supplementary Fig. 7b**). Conversely, the clusters identified in the filter found for responder patients were dominated by ICOS^{-} cell populations, including ICOS^{-}PD-1^{-} Tfh, ICOS^{-}PD-1^{-} memory cells, ICOS^{-}PD-1^{+} memory cells and naive T cells (**Fig. 8d, Supplementary Fig. 6c,d, Supplementary Fig. 7c**).

The difference in ICOS expression between patients that go on to be Abatacept responders *versus* non-responders is clear from a combined analysis of all cells contributing to clusters identified in both filters (**Fig. 8e**). Although overall PD-1 expression also differed between the two groups (**Fig. 8e**), its relationship with clinical response is more complex since certain PD-1^{+} populations are associated with a good response (e.g. ICOS^{-}PD-1^{+} memory) and others with a poor response (e.g. ICOS^{+}PD-1^{+} Tfh). Notably, both ICOS and PD-1 can influence Tfh migration and function[36, 37]. Analysis of Abatacept-treated mice showed that an analogous staining panel could be used to build a predictive model of clinical response with 84% accuracy and an AUC of 0.83 (**Supplementary Fig. 8a,b**). CellCnn identified filters that were enriched in mice that went on to be responders or non-responders, with ICOS being expressed at higher levels in the cells within the non-responder clusters (**Supplementary Fig. 8c,d,e**). Overall, both the predictive model and the CellCnn algorithm suggested that analysis of Tfh markers in baseline blood samples could predict clinical response following Abatacept immunotherapy.

Discussion

Heterogeneity in the response to costimulation inhibitors like Abatacept limits their utility as first line therapies, and therefore the ability to predict response to these reagents would have significant impact on how they are deployed. However, a fine-grained understanding of CD28-sensitive immune subsets, and their link to pathogenicity, has been lacking.

We show here that in both mice and humans experiencing ongoing autoimmune responses, costimulation blockade reduced Tfh frequencies, with principal component analysis identifying the loss of $CXCR5^+ICOS^+$ T cells as the biggest contributor to Abatacept-induced change. Since the majority of $CXCR5^+$ T cells are central memory cells[7, 28], it is plausible that the Abatacept-induced decrease in central memory T cells previously reported[32] reflects the loss of Tfh.

Importantly, we identified several new Abatacept-sensitive populations, including a population resembling Tph cells, thought to provide T cell help to B cells in the rheumatoid synovium[30]. Emerging data suggest these cells are expanded in children with islet autoantibodies who go on to develop diabetes[38], and are associated with disease activity in SLE[39] and RA[40, 41], suggesting insights into their drug sensitivity could have broad applicability. Furthermore, we found that cells resembling circulating Tfh precursors[27] also exhibit Abatacept sensitivity, as do a population of T cells expressing CD45RA and intermediate levels of ICOS. These could comprise recently activated T cells that have not yet lost CD45RA, or alternatively revertants that have lost, then re-expressed, this marker. Such revertants were first described in rodent models[42,43], where it was shown that they retained the capacity to provide B cell help[42]. $ICOS^+CD45RA^+$ T cells may therefore warrant further investigation in T-cell dependent autoimmune diseases featuring autoantibody production.

Tfh that remain post-Abatacept treatment exhibit an altered phenotype with a decrease in the frequency of Tfh expressing ICOS, PD-1 or both, and a reciprocal increase in Tfh expressing neither marker. The impact on ICOS expression appears dominant; accordingly, changes in $ICOS^+PD\text{-}1^-$ Tfh were a clear contributor to the Abatacept-induced variation in principal component analysis, while changes in $ICOS^-PD\text{-}1^+$ Tfh were not. The ability of CD28 signaling to promote ICOS expression is consistent with the original identification of ICOS as an "Inducible

306 Costimulator", responsive to CD28 engagement[44, 45]. Our new data suggest a continuous
307 requirement for CD28 signalling to sustain ICOS expression, implying that this hierarchy is
308 perpetuated even after T cell activation. Consistent with this, RNAseq analysis identified *Icos* to be
309 highly CD28-sensitive in human memory T cells[46].
310
311 ICOS signalling is critical for maintaining Tfh characteristics, with loss of ICOS permitting
312 upregulation of Klf2 and a reversion of Tfh phenotype[47]. Our data suggest that while CD28
313 blockade primarily inhibits early Tfh differentiation, prolonged CD28 blockade may effectively
314 inhibit ICOS signalling, by ensuring that remaining Tfh are ICOS-negative. Since ICOS is required
315 for Tfh maintenance, this may explain why CD28 blockade remains capable of decreasing Tfh
316 during an ongoing autoimmune response. Alternatively, the ability of CD28 blockade to inhibit
317 differentiation of new Tfh would lead to a decrease over time if turnover of Tfh was high.
318
319 Using gradient boosting, an ensemble machine learning method, on gated flow cytometry outputs
320 from pre-treatment samples, we were able to build a predictive model of Abatacept sensitivity that
321 could assign the clinical response at year 2 with 85% accuracy. There are two caveats to this model;
322 first, it is built on data from a relatively small number of patients and second, it intentionally
323 focuses on the best and worst responders. Thus, while it may work with high accuracy in these
324 patient groups, it may be less effective in individuals showing a borderline response.
325 Notwithstanding these caveats, the model highlights several T cell populations whose collective
326 frequencies appear to inform the clinical response to Abatacept. Chief among these is the
327 $ICOS^{+}$Tfh population, for which higher frequencies are associated with a poor clinical response.
328 Reciprocally, $ICOS^{-}PD\text{-}1^{-}$ Tfh contribute to the model, with a higher frequency being associated
329 with a better clinical response following Abatacept treatment.
330

Since Abatacept has only been trialled once in new onset T1D, we were unable to apply our predictive model to an independent dataset. We therefore sought an alternative means of validation. Using CellCnn we obtained independent corroboration for key aspects of our model. Notably this approach confirmed that a poor clinical response was associated with higher frequencies of $ICOS^+$ Tfh at baseline, while a good response was associated with higher frequencies of $ICOS^-PD\text{-}1^-$ Tfh. In addition, this analysis also revealed an effect of ICOS expression on CXCR5-negative cells. Thus, ICOS appears to be the most discerning cellular marker associated with preservation of beta-cell function following Abatacept treatment as assessed by two independent approaches, with data from a mouse model providing additional support.

Robust predictive markers of responsiveness to Abatacept are currently lacking, although there are suggestions that individuals with greater inflammatory activity exhibit a better clinical response[48]. A recent study using whole blood RNASeq detected changes in expression of B cell genes that were associated with clinical response in subjects with T1D treated with Abatacept[49], however these were not apparent until 84 days post treatment initiation. Since interventions that target Tfh inevitably alter B cell phenotype, it is tempting to speculate that such changes could be secondary to the altered T cell phenotypes observed here.

Our report is the first to suggest that baseline Tfh phenotypes have the potential to predict clinical response to an immunotherapy. It will be important to confirm these findings in a separate cohort of patients and to explore their wider applicability. For example, it remains to be established whether the T cell phenotypes we have identified can predict the response to Abatacept in other clinical settings, such as rheumatoid arthritis, or whether they are specific to T1D. Similarly, it will be important to ascertain whether these populations predict clinical response to other immunotherapies targeting costimulatory pathways or T cell / B cell collaboration. Broader implications aside, the

incorporation of Tfh analysis could alter the landscape for the rational use of Abatacept and novel versions of this molecule with improved affinity, stability and pharmacokinetics that are emerging.

Acknowledgements

This work was funded by Diabetes UK, MedImmune Ltd (now AstraZeneca plc), the Medical Research Council, and the Rosetrees Trust. The authors received funding from the European Union's Horizon 2020 research and innovation programme under the Marie Sklodowska-Curie grant agreement No 675395. Diabetes research in the Walker lab is supported by Type One Mission. We acknowledge the support of the Type 1 Diabetes TrialNet Study Group, which identified study participants and provided samples and follow-up data for this study. The Type 1 Diabetes TrialNet Study Group is a clinical trials network funded by the National Institutes of Health (NIH) through the National Institute of Diabetes and Digestive and Kidney Diseases, the National Institute of Allergy and Infectious Diseases, and The Eunice Kennedy Shriver National Institute of Child Health and Human Development, through the cooperative agreements U01 DK061010, U01 DK061016, U01 DK061034, U01 DK061036, U01 DK061040, U01 DK061041, U01 DK061042, U01 DK061055, U01 DK061058, U01 DK084565, U01 DK085453, U01 DK085461, U01 DK085463, U01 DK085466, U01 DK085499, U01 DK085505, U01 DK085509, and JDRF. The contents of this article are solely the responsibility of the authors and do not necessarily represent the official views of the NIH or JDRF. We thank A. Pesenacker for helpful comments on the manuscript.

Author contributions

N.M.E. performed experiments, analysed data, prepared figures and co-wrote the manuscript. F.H. performed experiments, analysed data and edited the manuscript. N.T. performed predictive

modelling, prepared figures and co-wrote the manuscript. C.J.W., L.P., R.K., A.K., V.O., E.M.R., E.N., Y.E., M.E., and R.B., assisted with experiments and edited the manuscript. P.A., and L.J., provided expertise and funding. M.P. provided expertise and facilitated sample sharing. M.R. provided expertise and was co-applicant for funding. L.S.K.W. conceptualised and supervised the study, applied for funding and wrote the manuscript.

Competing interests

AstraZeneca plc contributed to the funding of the study. P.A. and L.J. declare an interest in developing costimulation blockade reagents at AstraZeneca plc. L.S.K.W. and N.T. are inventors on a patent application related to these findings.

References

1. Blair, H.A. & Deeks, E.D. Abatacept: A Review in Rheumatoid Arthritis. *Drugs* **77**, 1221-1233 (2017).

2. Mease, P.J. *et al.* Efficacy and safety of abatacept, a T-cell modulator, in a randomised, double-blind, placebo-controlled, phase III study in psoriatic arthritis. *Ann Rheum Dis* **76**, 1550-1558 (2017).

3. Brunner, H.I. *et al.* Subcutaneous Abatacept in Patients With Polyarticular-Course Juvenile Idiopathic Arthritis: Results From a Phase III Open-Label Study. *Arthritis & rheumatology* **70**, 1144-1154 (2018).

4. Lenschow, D.J. *et al.* Differential effects of anti-B7-1 and anti-B7-2 monoclonal antibody treatment on the development of diabetes in the nonobese diabetic mouse. *The Journal of experimental medicine* **181**, 1145-1155 (1995).

5. Orban, T. *et al.* Co-stimulation modulation with abatacept in patients with recent-onset type 1 diabetes: a randomised, double-blind, placebo-controlled trial. *Lancet* **378**, 412-419 (2011).

6. Orban, T. *et al.* Costimulation modulation with abatacept in patients with recent-onset type 1 diabetes: follow-up 1 year after cessation of treatment. *Diabetes Care* **37**, 1069-1075 (2014).

7. Kenefeck, R. *et al.* Follicular helper T cell signature in type 1 diabetes. *Journal of Clinical Investigation* **125**, 292-303 (2015).

8. Yu, D. *et al.* The transcriptional repressor Bcl-6 directs T follicular helper cell lineage commitment. *Immunity* **31**, 457-468 (2009).

9. Johnston, R.J. *et al.* Bcl6 and Blimp-1 are reciprocal and antagonistic regulators of T follicular helper cell differentiation. *Science* **325**, 1006-1010 (2009).

10. Nurieva, R.I. *et al.* Bcl6 mediates the development of T follicular helper cells. *Science* **325**, 1001-1005 (2009).

11. Heit, A. *et al.* Vaccination establishes clonal relatives of germinal center T cells in the blood of humans. *J Exp Med* **214**, 2139-2152 (2017).

12. Hill, D.L. *et al.* The adjuvant GLA-SE promotes human Tfh cell expansion and emergence of public TCRbeta clonotypes. *J Exp Med* **8** 1857-1873 (2019).

13. Schmitt, N., Bentebibel, S.E. & Ueno, H. Phenotype and functions of memory Tfh cells in human blood. *Trends in Immunology* **35**, 436-442 (2014).

14. Sage, P.T., Alvarez, D., Godec, J., von Andrian, U.H. & Sharpe, A.H. Circulating T follicular regulatory and helper cells have memory-like properties. *Journal of Clinical Investigation* **12**, 5191-204 (2014).

15. Xu, X. *et al.* Inhibition of increased circulating Tfh cell by anti-CD20 monoclonal antibody in patients with type 1 diabetes. *PLoS One* **8**, e79858 (2013).

16. Ferreira, R.C. *et al.* IL-21 production by CD4 effector T cells and frequency of circulating follicular helper T cells are increased in type 1 diabetes patients. *Diabetologia* **58**, 781-790 (2015).

17. Serr, I. *et al.* miRNA92a targets KLF2 and the phosphatase PTEN signaling to promote human T follicular helper precursors in T1D islet autoimmunity. *Proc Natl Acad Sci U S A* **113**, E6659-E6668 (2016).

18. Viisanen, T. *et al.* Circulating CXCR5+PD-1+ICOS+ Follicular T Helper Cells Are Increased Close to the Diagnosis of Type 1 Diabetes in Children With Multiple Autoantibodies. *Diabetes* **66**, 437-447 (2017).

19. Borriello, F. *et al.* B7-1 and B7-2 have overlapping, critical roles in immunoglobulin class switching and germinal center formation. *Immunity* **6**, 303-313 (1997).

20. Walker, L.S. *et al.* Compromised OX40 function in CD28-deficient mice is linked with failure to develop CXCR5-positive CD4 cells and germinal centers. *J Exp Med* **190**, 1115-1122 (1999).

21. Wang, C.J. *et al.* CTLA-4 controls follicular helper T-cell differentiation by regulating the strength of CD28 engagement. *Proc Natl Acad Sci U S A* **112**, 524-529 (2015).

22. Verstappen, G.M. *et al.* Attenuation of Follicular Helper T Cell-Dependent B Cell Hyperactivity by Abatacept Treatment in Primary Sjogren's Syndrome. *Arthritis & rheumatology* **69**, 1850-1861 (2017).

23. Piantoni, S., Regola, F., Scarsi, M., Tincani, A. & Airo, P. Circulating follicular helper T cells (CD4+CXCR5+ICOS+) decrease in patients with rheumatoid arthritis treated with abatacept. *Clin Exp Rheumatol* **36**, 685 (2018).

24. Glatigny, S. *et al.* Abatacept Targets T Follicular Helper and Regulatory T Cells, Disrupting Molecular Pathways That Regulate Their Proliferation and Maintenance. *J Immunol* (2019).

25. Clough, L.E. *et al.* Release from Regulatory T Cell-Mediated Suppression during the Onset of Tissue-Specific Autoimmunity Is Associated with Elevated IL-21. *J Immunol* **180**, 5393-5401 (2008).

26. Walker, L.S., Chodos, A., Eggena, M., Dooms, H. & Abbas, A.K. Antigen-dependent proliferation of CD4+ CD25+ regulatory T cells in vivo. *J Exp Med* **198**, 249-258 (2003).

27. He, J. *et al.* Circulating precursor CCR7(lo)PD-1(hi) CXCR5(+) CD4(+) T cells indicate Tfh cell activity and promote antibody responses upon antigen reexposure. *Immunity* **39**, 770-781 (2013).

28. Morita, R. *et al.* Human blood CXCR5(+)CD4(+) T cells are counterparts of T follicular cells and contain specific subsets that differentially support antibody secretion. *Immunity* **34**, 108-121 (2011).

29. Arvaniti, E. & Claassen, M. Sensitive detection of rare disease-associated cell subsets via representation learning. *Nature communications* **8**, 14825 (2017).

30. Rao, D.A. *et al.* Pathologically expanded peripheral T helper cell subset drives B cells in rheumatoid arthritis. *Nature* **542**, 110-114 (2017).

31. Pieper, J. *et al.* CTLA4-Ig (abatacept) therapy modulates T cell effector functions in autoantibody-positive rheumatoid arthritis patients. *BMC Immunol* **14**, 34 (2013).

32. Orban, T. *et al.* Reduction in CD4 central memory T-cell subset in costimulation modulator abatacept-treated patients with recent-onset type 1 diabetes is associated with slower C-peptide decline. *Diabetes* **63**, 3449-3457 (2014).

33. Leete, P. *et al.* Differential Insulitic Profiles Determine the Extent of beta-Cell Destruction and the Age at Onset of Type 1 Diabetes. *Diabetes* **65**, 1362-1369 (2016).

34. Breiman, L. Arcing the edge. *Technical Report 486* **Dept. Statistics, Univ. California, Berkeley. Available at www.stat.berkeley.edu** (1997).

35. Friedman, J.H. Greedy Function Approximation: A Gradient Boosting Machine. *Technical Report* **Dept. Statistics, Stanford University** (1999).

36. Xu, H. *et al.* Follicular T-helper cell recruitment governed by bystander B cells and ICOS-driven motility. *Nature* **496**, 523-527 (2013).

37. Shi, J. *et al.* PD-1 Controls Follicular T Helper Cell Positioning and Function. *Immunity* **49**, 264-274 e264 (2018).

38. Ekman, I. *et al.* Circulating CXCR5(-)PD-1(hi) peripheral T helper cells are associated with progression to type 1 diabetes. *Diabetologia* **62**, 1681-1688 (2019).

39. Bocharnikov, A.V. *et al.* PD-1hiCXCR5- T peripheral helper cells promote B cell responses in lupus via MAF and IL-21. *JCI insight* **4** (2019).

40. Zhang, F. *et al.* Defining inflammatory cell states in rheumatoid arthritis joint synovial tissues by integrating single-cell transcriptomics and mass cytometry. *Nat Immunol* (2019).

41. Fortea-Gordo, P. *et al.* Two populations of circulating PD-1hiCD4 T cells with distinct B cell helping capacity are elevated in early rheumatoid arthritis. *Rheumatology (Oxford)* **58**, 1662-1673 (2019).

42. Bell, E.B. *et al.* Both CD45R(low) and CD45R(high) "revertant" CD4 memory T cells provide help for memory B cells. *Eur J Immunol* **31**, 1685-1695 (2001).

43. Merica, R., Khoruts, A., Pape, K.A., Reinhardt, R.L. & Jenkins, M.K. Antigen-experienced CD4 T cells display a reduced capacity for clonal expansion in vivo that is imposed by factors present in the immune host. *J Immunol* **164**, 4551-4557 (2000).

44. Hutloff, A. *et al.* ICOS is an inducible T-cell co-stimulator structurally and functionally related to CD28. *Nature* **397**, 263-266 (1999).

45. McAdam, A.J. *et al.* Mouse inducible costimulatory molecule (ICOS) expression is enhanced by CD28 costimulation and regulates differentiation of CD4+ T cells. *J Immunol* **165**, 5035-5040 (2000).

46. Glinos, D.A., Soskic, B., Jostins, L., Sansom, D.M. & Trynka, G. Genomic profiling of T cell activation reveals dependency of memory T cells on CD28 costimulation. *Preprint at https://www.biorxiv.org/content/biorxiv/early/2018/09/18/421099.full.pdf* (2019).

47. Weber, J.P. *et al.* ICOS maintains the T follicular helper cell phenotype by down-regulating Kruppel-like factor 2. *J Exp Med* **212**, 217-233 (2015).

48. Cabrera, S.M. *et al.* Innate immune activity as a predictor of persistent insulin secretion and association with responsiveness to CTLA4-Ig treatment in recent-onset type 1 diabetes. *Diabetologia* **61**, 2356-2370 (2018).

49. Linsley, P.S., Greenbaum, C.J., Speake, C., Long, S.A. & Dufort, M.J. B lymphocyte alterations accompany abatacept resistance in new-onset type 1 diabetes. *JCI insight* **4** (2019).

Figure Legends

Figure 1. Time-sensitive inhibition of Tfh by Abatacept in immunised mice

DO11.10 T cells (2 x 10^5) were injected i.v. into *Cd28*$^{-/-}$ mice that were immunised i.p. with 200 µg of OVA/alum 24 h later. Abatacept or Control-Ig were administered i.p. every two to three days starting at the indicated time points. Control-Ig treatment was initiated at d-1. At day 7 after immunisation, spleens were harvested for analysis. (**a**) Representation of treatment scheme. (**b**) Representative flow cytometry plots for CXCR5$^+$PD-1$^+$ Tfh cells in gated CD4$^+$DO11.10$^+$ cells (top) and Fas$^+$GL7$^+$ GC B cells in gated CD19$^+$ cells (bottom). (**c**) Collated data for Tfh cells, GC B cells, and CD40L and ICOS frequencies in gated CD4$^+$DO11.10$^+$ cells. (**d**) Collated data for absolute numbers of DO11.10$^+$ Tfh, GC B cells, CD40L$^+$CD4$^+$DO11.10$^+$ cells and ICOS$^+$CD4$^+$DO11.10$^+$ cells. Data are compiled from five independent experiments; n=6 mice unimmunised, 10 mice Control-Ig, 12 mice Abatacept d-1, 11 mice each Abatacept d2 and Abatacept d4. Mean + SD are shown. (**c**) and (**d**) Kruskal-Wallis test for multiple comparisons followed by pairwise two-tailed Mann-Whitney U test with Bonferroni correction; ****, $p < 0.0001$; ***, $p < 0.001$; **, $p < 0.01$; *, $p < 0.05$; ns, not significant.

Figure 2. Abatacept decreases Tfh during an ongoing autoimmune response in mice

Abatacept or Control-Ig were injected every two to three days i.p. into 6-8 week old DO11.10 x RIP-mOVA mice. At day 11, pancreas-draining lymph nodes (panLN) and spleens were harvested for analysis. (**a**) Representation of treatment scheme. (**b,c**) Collated data for frequencies (**b**) and absolute numbers (**c**) of Tfh cells in gated CD4$^+$ cells. Data are compiled from two independent experiments; n=10 mice in each treatment group. Mean + SD are shown. Two-tailed Mann-Whitney U test; ***, $p < 0.001$; **, $p < 0.01$.

Figure 3. Abatacept decreases Tfh in patients with new onset type 1 diabetes

599 Frozen PBMC samples from patients with recent onset T1D that received Abatacept or placebo
600 were thawed and stained for flow cytometry analysis. Samples were taken at baseline, one year and
601 two years after treatment initiation. (**a**) Collated data for Tfh ($CD45RA^{-}CXCR5^{+}$) frequencies in
602 $CD3^{+}CD4^{+}$ cells from recipients of Abatacept (left) or placebo (right). (**b**) Principal component
603 analysis on population frequencies obtained from flow cytometry analysis. Analysis was performed
604 on all samples simultaneously and split into treatment groups for visualisation purposes. (**c**)
605 Contributions of individual populations to PC1. (**d**) Collated data for $ICOS^{+}PD\text{-}1^{+}$ and $CCR7^{-}PD\text{-}$
606 1^{+} frequencies in $CD4^{+}CD45RA^{-}CXCR5^{+}$ cells. Shown are boxplots with black horizontal line
607 denoting median value, while box represents interquartile ranges (IQR, Q1-Q3 percentile) and
608 whiskers show minimum (Q1– 1.5 * IQR) and maximum (Q3 + 1.5 * IQR) values. Abatacept, n =
609 34 patients; Placebo, n = 13 patients (Year 1) or 14 patients (Baseline and Year 2). Two-tailed
610 Wilcoxon signed-rank test; ****, $p < 0.0001$; ns, not significant.
611
612 **Figure 4. Data-driven analysis reveals additional Abatacept-sensitive populations in type 1**
613 **diabetes patients**
614 CellCnn analysis followed by k-means clustering of filter-specific cells was applied to flow
615 cytometry data of samples taken at baseline and two years after Abatacept or placebo treatment
616 initiation. (**a**) Frequency of filter specific cells in each analysed sample. (**b**) t-SNE projection of
617 down-sampled, pooled flow cytometry data of all samples used for CellCnn analysis. K-means
618 clusters of filter-specific cells are highlighted. (**c**) Representative flow cytometry overlays of
619 cluster-specific cells (colour) on original flow cytometry data (grey). Examples shown are from a
620 baseline sample. (**d**) Frequency of cluster-specific cells in each analysed sample. (**e**) Collated data
621 for frequency of manually gated T-peripheral helper cells ($ICOS^{+}PD\text{-}1^{+}CXCR5^{-}CD45RA^{-}$ in
622 $CD4^{+}CD3^{+}$). Abatacept, n = 34 patients; Placebo, n = 13 patients (Year 1) or 14 patients (Baseline
623 and Year 2). In (**a**) and (**d**) boxplots are shown with black horizontal line denoting median value,
624 while box represents interquartile ranges (IQR, Q1-Q3 percentile) and whiskers show minimum

(Q1– 1.5 * IQR) and maximum (Q3 + 1.5 * IQR) values. Two-tailed Wilcoxon signed-rank test; ****, $p < 0.0001$; ns, not significant.

Figure 5. "Tph" and "ICOS$^+$ naive" cells are elevated in a mouse model of diabetes and sensitive to costimulation blockade

Cells isolated from panLN and spleens were stained with a panel of markers to identify Tph ($CD4^+CD45RB^-CXCR5^-ICOS^+PD\text{-}1^+$) and $ICOS^+$ naive T cells ($CD4^+CD45RB^+ICOS^+$). Representative flow cytometry plots for gating strategy of Tph (**a**) and $ICOS^+$ naive T cells (**d**) in spleen. Collated data for frequencies (top) and absolute numbers (bottom) of Tph (**b**) and $ICOS^+$ naive T cells (**e**) in panLN (left) and spleen (right) of DO11.10 and DO11.10 x RIP-mOVA mice. (**c,f**) DO11.10 x RIP-mOVA mice were treated with Abatacept and Control-Ig according to treatment scheme depicted in **Fig. 2a**. Shown are collated data for frequencies (top) and absolute numbers (bottom) of Tph (**c**) and $ICOS^+$ naive T cells (**f**) in panLN (left) and spleen (right). Data are compiled from 2 (**c, f**), 3 (**b**) or 4 (**e**) independent experiments; n=6 (**b**), 7 (**e**) or 9 (**c, f**) mice. Mean + SD are shown. Two-tailed Mann-Whitney U test; ****, $p < 0.0001$; ***, $p < 0.001$; **, $p < 0.01$; *, $p < 0.05$.

Figure 6. Tph cells identified through CellCnn display marker expression consistent with a Tph profile

Frozen PBMC samples from recent onset T1D patients that received Abatacept or placebo were thawed and analysed by flow cytometry for Tph and Tfh markers. (**a**) Representative gating strategy for CXCR5 vs PD-1 populations (left) and Tph previously identified through CellCnn analysis (right). (**b**) Collated data for frequency of cells in the CellCnn 'Tph' gate. (**c**) Expression of Tph markers on "Tph" identified by CellCnn compared with classically identified $CXCR5^-PD1^{hi}$ Tph gated as shown in (**a**). Data was obtained from baseline samples and shown are mean + SD. (**d, e**) CellCnn analysis of samples identifies a cluster of Tph-phenotype cells. Shown is expression of

651 indicated markers within cluster (green) and all cells (grey) of representative sample (**d**) and
652 frequency of cluster-specific cells in Abatacept- or Placebo-treated T1D patients (**e**). (**b, e**)
653 Abatacept, n=15 (Baseline) or 20 (Year 1 and Year 2) patients; Placebo, n=6 (Baseline) or 8 (Year
654 1 and Year 2) patients; (**c**) n=21 patients. In (**b**) and (**e**) boxplots are shown with black horizontal
655 line denoting median value, while box represents interquartile ranges (IQR, Q1-Q3 percentile) and
656 whiskers show minimum (Q1– 1.5 * IQR) and maximum (Q3 + 1.5 * IQR) values. Two-tailed
657 Mann-Whitney U test; ****, $p < 0.0001$; ***, $p < 0.001$; **, $p < 0.01$; *, $p < 0.05$; ns, not
658 significant.
659
660 **Figure 7. Baseline Tfh phenotype is associated with clinical response to Abatacept**
661 (**a**) C-peptide AUC (as % of screening C-peptide AUC) of placebo treated and top 10 (at day 728)
662 responder and non-responder Abatacept-treated patients. Responder, n=9 (D196, D364, D560) or
663 10 (all other time points) patients; Non-Responder, n=9 (D364, D560) or 10 (all other time points)
664 patients; Placebo, n=13 (D196) or 14 (all other time points) patients. (**b**) A gradient boosting model
665 was constructed using nested leave-one-out cross validation to predict clinical response following
666 Abatacept treatment. ROC curve of the predictive model is shown. (**c**) Features ranked by
667 importance for predicting clinical response following Abatacept treatment. Bar shows mean and
668 black lines represent 95% confidence intervals, n=20 patients. (**d**) Frequencies of indicated flow
669 cytometry gated populations at baseline (n=10 patients in each group). In (**a**) and (**d**) boxplots are
670 shown with black horizontal line denoting median value, while box represents interquartile ranges
671 (IQR, Q1-Q3 percentile) and whiskers show minimum (Q1– 1.5 * IQR) and maximum (Q3 + 1.5 *
672 IQR) values. (**a**) Two-way ANOVA with Bonferroni correction; (**d**) Two-tailed Mann-Whitney U
673 test; ****, $p < 0.0001$; ***, $p < 0.001$; **, $p < 0.01$; *, $p < 0.05$; ns, not significant.
674
675 **Figure 8. Data-driven analysis identifies cell signatures linked to clinical response to**
676 **Abatacept**

CellCnn analysis followed by k-means clustering of filter-specific cells was applied to flow cytometry data of samples taken at baseline from top 10 responder and non-responder Abatacept treated patients. (**a**) t-SNE projection of down-sampled, pooled flow cytometry data of all samples used for CellCnn analysis. Filter-specific cells for responder and non-responder filter are highlighted. (**b**) Frequencies of filter-specific cells in each sample for responder and non-responder filter. (**c**) Frequencies and representative flow cytometry overlays for clusters found in non-responder filter-specific cells. (**d**) Frequencies and representative flow cytometry overlays for clusters found in responder filter-specific cells. (**e**) Histograms of marker expression of filter-specific cells (yellow; non-responder, blue; responder) or all cells (grey). n=10 patients in each group. In (**b**), (**c**) and (**d**) boxplots are shown with black horizontal line denoting median value, while box represents interquartile ranges (IQR, Q1-Q3 percentile) and whiskers show minimum (Q1– 1.5 * IQR) and maximum (Q3 + 1.5 * IQR) values. (**b**), (**c**) and (**d**) two-tailed Mann–Whitney U test; (**e**) two-tailed Kolmogorov-Smirnov (ks) test; **, $p < 0.01$; *, $p < 0.05$. All representative overlay plots are from the same baseline sample.

Methods

Patients

Cryopreserved PBMC samples from a clinical trial (NCT00505375) that has previously been published[5] were provided by Type 1 Diabetes TrialNet as part of the Effects of CTLA-4 IG (Abatacept) on the Progression of Type 1 Diabetes in New Onset Subjects (TN-09) study. Briefly, in this study individuals with recent onset T1D (diagnosed within the past 100 days) were randomised to receive CTLA4-Ig (Abatacept) (10mg/kg) or placebo (saline) intravenously on days 1, 14, 28 and subsequently once monthly for 2 years. The protocol and consent document of this trial were approved by appropriate independent ethics committees or institutional review boards. All participants (or parents) provided written, informed consent; in addition to their parents providing consent, participants younger than 18 years of age signed a study assent form Samples were provided from study participants at the time of screening and 12 and 24 months following treatment initiation. Data from 36 Abatacept-treated and 14 placebo-treated patients were acquired. Samples from two Abatacept-treated individuals were excluded from the analysis due to low data quality. For one placebo-treated patient, no 12-month sample was acquired. Samples were supplied in a blinded and randomised way in two batches separated by a break of 9 months. A further set of samples from 20 Abatacept-treated and 8 placebo-treated patients were obtained and analysed during revision of the manuscript (**Fig. 6, Fig. S3**). Demographic and clinical data were only provided following submission of raw data files to TrialNet. To assess stimulated C-peptide secretion, four-hour mixed meal tolerance tests (MMTTs) were performed at screening and at 24 months. Additional two-hour MMTTs were conducted at 3, 6, 12 and 18 months, although for some patients C-peptide data was not available for all timepoints. For comparison across all timepoints only the first 2 hours of the 4-hour MMTTs were used.

Mice

BALB/c DO11.10 TCR transgenic mice were obtained from The Jackson Laboratory and BALB/c *Cd28*$^{-/-}$ mice from Taconic Laboratories. BALB/c RIP-mOVA mice (expressing the ovalbumin transgene under control of the rat insulin promoter, from line 296-1B) were a gift from W. Heath (Doherty Institute, Melbourne, Australia). DO11.10 mice were crossed with RIP-mOVA mice to generate DO11.10 x RIP-mOVA mice. Mice were housed according to Home Office guidelines in individually vented cages with environmental enrichment (e.g. cardboard tunnels, paper houses, chewing blocks) in a temperature and humidity-controlled facility with a 14 h light–10 h dark cycle and ad libitum feeding at University College London Biological Services Unit. Experiments were performed in accordance with the relevant Home Office project and personal licenses following approval from the University College London Animal Welfare Ethical Review Body.

In Vivo Experiments

For adoptive transfer experiments, 2 x10^5 T cells from DO11.10 mice were injected i.v. into *Cd28*$^{-/-}$ recipients. 24h later, recipients were immunised i.p. with 200 µg of OVA/alum (Sigma). Where indicated mice were injected i.p. with 500 µg Abatacept (Royal Free Hospital Pharmacy) or control antibody (human IgG1, BioXCell) at the same time as adoptive transfer (d-1). Subsequently, mice received 250 µg Abatacept or control antibody every 2-3 days over the course of the experiment (see **Fig. 1a**). For experiments using DO11.10 x RIP-mOVA mice, 6-13 week old animals were injected i.p. with 500 µg Abatacept or control antibody. Mice were subsequently treated with 250 µg Abatacept or control antibody every 2-3 days over a period of 11 days. For experiments in **Fig. S8**, DO11.10 x RIP-mOVA mice with a blood glucose reading between 180 and 290 mg/dL were injected i.p. with Abatacept, 500 µg for the initial dose then 250 µg three times weekly, for four weeks and blood glucose was monitored. Mouse spleen and lymph nodes were mashed to create single cell suspensions and 2-10 x 10^6 cells were used for flow cytometry staining. All injections were carried out in the absence of anesthesia and analgesia, and mice were returned immediately to home cages following the procedure. The welfare of experimental animals

748 was monitored regularly (typically immediately post procedure, then at least every 2–3 days). No
749 unexpected adverse events were noted during the course of these experiments.
750
751 **Human sample preparation**
752 Cryopreserved samples were thawed in a 37°C water bath and vial contents transferred to a 15 mL
753 Falcon tube. Pre-warmed defrost media (RPMI (Glutamax with HEPES) (Life Technologies
754 (Thermo Fisher)), 5% human AB serum (Sigma), 20 nM TAPI-2 (Sigma), 50 U/mL Benzonase
755 (Sigma) was added dropwise to 10 mL. Cells were rested in 4 mL resting media (RPMI with 10%
756 human AB serum, 20 nM TAPI-2) for 1 hour at 37°C. 2 x 10^6 cells were used for subsequent flow
757 cytometry staining.
758
759 **Flow Cytometry**
760 Mouse cells were surface stained with Fas PE (BD Biosciences, clone: Jo2, 1/50), CD19 BUV395
761 (BD Biosciences, clone: 1D3, 1/50), CD4 BUV395 (BD Biosciences, clone: GK1.5, 1/100), CD4
762 PerCP-Cy5.5 (BD Biosciences, clone: RM4-5, 1/100), GL7 AlexaFluor 488 (Biolegend, clone:
763 GL7, 1/200), CXCR5 BV421 (Biolegend, clone: L138D7, 1/20), PD-1 PE-Cy7 (Biolegend, clone:
764 RMP1-30, 1/50), ICOS PE (eBioscience (Thermo Fisher), clone: 7E.17G9, 1/100), CD45 BUV395
765 (BD Biosciences, clone: 30-F11, 1/100), CD45RB APC (used in mouse panels in place of
766 CD45RA, eBioscience (Thermo Fisher), clone: C363.16A, 1/100) and DO11.10 TCR APC
767 (eBioscience (Thermo Fisher), clone: KJ126, 1/100) for 30 minutes at 4°C. Cells were fixed and
768 permeabilised using the Foxp3/Transcription Factor Staining Buffer Set (eBioscience (Thermo
769 Fisher)) and stained intracellularly with CD40L PE (BD Biosciences, clone: MR1, 1/100) for 30
770 minutes at 4°C. For experiments involving Abatacept blockade in DO11.10 x RIP-mOVA mice,
771 cells were stained with fixable viability dye eFluor 780 (eBioscience (Thermo Fisher)) in PBS for
772 10 minutes at 4°C. After washing once with PBS containing 2% fetal calf serum, samples were
773 preincubated with purified anti-CD16/32 (BD Biosciences, clone: 2.4G2, 1 μL) for 5 minutes at

774 37°C. In **Fig. S8**, mouse cells were preincubated with purified anti-CD16/32 for 5 minutes at 37°C
775 and stained with CXCR5 BV421 for 30 minutes at 37°C. Subsequently, an antibody cocktail
776 containing CD3 BUV395 (BD Biosciences, clone: 145-2C11, 1/50), CD4 PerCP-Cy5.5, CD45RB
777 APC, CCR7 AlexaFluor 488 (Biolegend, clone: 4B12, 2.5 µL), PD-1 PE-Cy7, ICOS PE, CD25 PE-
778 Cf594 (BD Biosciences, clone: PC61, 1/200) and fixable viability dye eFluor 780 was added and
779 cells were incubated for 30 minutes at 37°C.
780 Human cells were washed once in PBS and stained for 15 minutes at 37°C with CCR7 BV605
781 (Biolegend, clone: G043H7, 3 µL) in Brilliant Stain Buffer (BD Biosciences). An antibody cocktail
782 containing CD3 BUV395 (BD Biosciences, clone: SK7, 3 µL), CD4 PE-Cy7 (BD Biosciences,
783 clone: SK3, 3 µL), CD25 BV421 (BD Biosciences, clone: M-A251, 3 µL), CD45RA PerCP-Cy5.5
784 (eBioscience (Thermo Fisher), clone: HI100, 1 µL), CD62L AlexaFluor 700 (Biolegend, clone:
785 DREG-56, 3 µL), CD127 BV711 (BD Biosciences, clone: HIL-7R-M21, 3 µL), CXCR5
786 AlexaFluor 488 (BD Biosciences, clone: RF8B2, 5 µL), PD-1 PE (eBioscience (Thermo Fisher),
787 clone: ebioJ105, 3 µL) and ICOS biotin (eBioscience (Thermo Fisher), clone: ISA-3, 3 µL) was
788 subsequently added and cells were incubated for another 15 minutes at 4°C. Cells were then washed
789 in PBS, streptavidin APC (BD Biosciences, 2 µL) was added to the residual volume and cells were
790 incubated for 10 minutes at 4°C. Cells were resuspended in fixable viability dye eFluor 780 in PBS
791 and incubated for 10 minutes at 4°C before being washed in PBS twice. Due to technical issues
792 with CD62L staining this marker was not considered in any of the downstream analysis. In **Fig. 6**,
793 human cells were sequentially stained with CCR2 BV510 (Biolegend, clone: K036C2, 3 µL), CCR5
794 BUV737 (BD Biosciences, clone: 2D7, 1 µL) and CCR7 BV605 at 37°C for 30, 20 and 15 minutes,
795 respectively. Subsequently, an antibody cocktail containing CD3 BUV395, CD4 PE-Cy7, CXCR5
796 AlexaFluor 488, CD45RA PerCP-Cy5.5, HLA-DR BV785 (Biolegend, clone: L243, 3 µL), CD38
797 PE-Cf594 (BD Biosciences, HIT2, 1 µL), TIGIT BV421 (Biolegend, clone: A15153G, 3 µL) and
798 BTLA BV650 (BD Biosciences, clone: J168-540, 2 µL) was added and cells were incubated for 15
799 minutes at 4°C. In **Fig. S3**, human cells were stained with CD3 BUV395, CD4 PE-Cy7, CXCR5

AlexaFluor 488, CD45RA PerCP-Cy5.5, CXCR3 BV785 (Biolegend, clone: G025H7, 3 μL) and CCR6 APC-R700 (BD Biosciences, clone: 11A9, 3 μL) for 15 minutes at 4°C.

All data was acquired on a BD LSRFortessa (BD Biosciences) using BD FACSDiva (BD Biosciences). For manual analysis, data was analysed using FlowJo software version 10. For automated analysis, data was pre-gated on live $CD3^{+}CD4^{+}$ cells in FlowJo, loaded into R using the Bioconductor package flowCore and underwent quality control using Bioconductor package FlowAI with standard configurations[50]. Low-quality events were removed and marker expression was transformed using arcsinh transformation using the Bioconductor package flowVS. CellCnn was run using a filter difference threshold of 0.5, maximum epochs of 100 and otherwise standard configurations. Filter specific cells were identified as cells having a filter response value in the upper 5% of the overall filter response. K-means clustering was performed using the CRAN package Stats, and optimal number of clusters were chosen using the Elbow method. Cluster information was added to fcs files using Bioconductor packages CytoML and flowWorkspace. The CRAN package Rtsne was used to compute t-SNE.

Statistics and Predictive Modelling

Statistical analysis was performed using R v3.5.1 and Python v3.7. Two-sided Mann–Whitney U was used for comparison of two unpaired means. For comparison of paired means two-sided Wilcoxon signed-rank test was used. Comparison of more than two means was performed using two-sided ANOVA or Kruskal-Wallis test with Bonferroni correction. Equality of histograms in Fig. 6e and Fig. S8e was assessed using the Kolmogorov-Smirnov test. Normality was tested using Shapiro-Wilk test and homogeneity of variance was tested using Levene's test. All measurements were taken from distinct samples. For boxplots, the black horizontal line indicates the median, the boxes represent interquartile range (IQR, Q1-Q3 percentile) and whiskers show minimum (first quartile - 1.5 * IQR) and maximum (third quartile $^{+}$ 1.5 * IQR). Principal component analysis was performed on scaled and centered data. Plots were produced using either CRAN packages ggplot2,

ggpubr, ggsignif, RColourBrewer and scales in R or matplotlib and seaborn in Python. All predictive modelling was conducted using Python v3.7. Data cleaning and formatting was carried out using either CRAN packages plyr, stringr and tidyr in R or pandas and numpy in Python. The gradient boosting algorithm was implemented using sklearn. Feature correlation was calculated using Pearson's r to ensure that the model did not contain sets of highly correlated variables which can make predictions unstable and dilute feature importance effects. Feature pairs which were correlated with r>=0.95 were determined, and only the most predictive feature of each pair was included in the gradient boosting model.

Code Availability

Computer code is available from the corresponding author on request.

Data Availability

The authors declare that the data supporting the findings of this study are available within the paper and its supplementary information files.

Methods-only References

50. Monaco, G. *et al.* flowAI: automatic and interactive anomaly discerning tools for flow cytometry data. *Bioinformatics* **32**, 2473-2480 (2016).

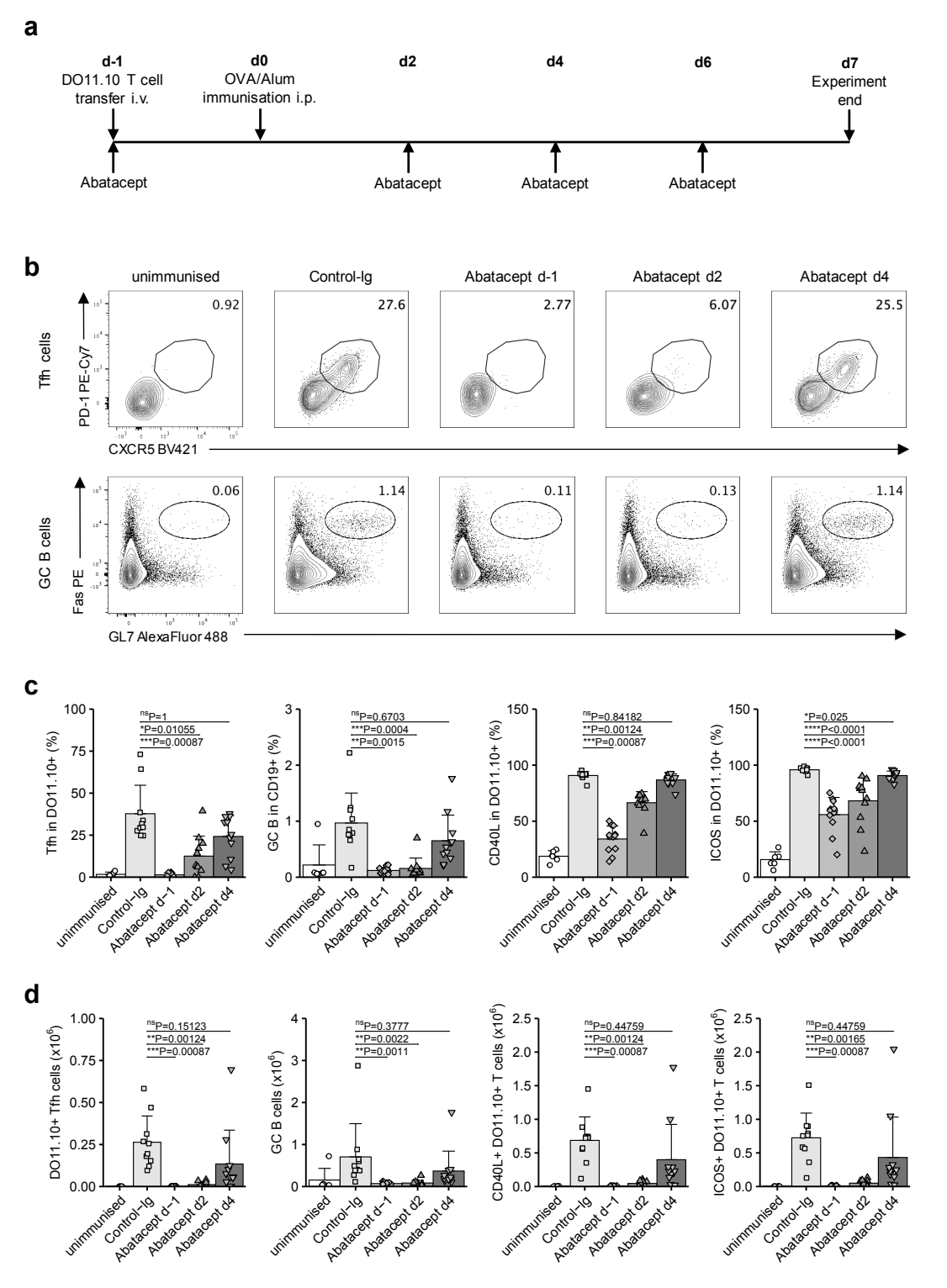
a
d-1
DO11.10 T cell transfer i.v.
d0
OVA/Alum immunisation i.p.
d2
d4
d6
d7
Experiment end
Abatacept
Abatacept
Abatacept
Abatacept
b
unimmunised
Control-Ig
Abatacept d-1
Abatacept d2
Abatacept d4
Tfh cells
PD-1 PE-Cy7
CXCR5 BV421
0.92
27.6
2.77
6.07
25.5
GC B cells
Fas PE
GL7 AlexaFluor 488
0.06
1.14
0.11
0.13
1.14
c
Tfh in DO11.10+ (%)
nsP=1
*P=0.01055
***P=0.00087
GC B in CD19+ (%)
nsP=0.6703
***P=0.0004
**P=0.0015
CD40L in DO11.10+ (%)
nsP=0.84182
**P=0.00124
***P=0.00087
ICOS in DO11.10+ (%)
*P=0.025
****P<0.0001
****P<0.0001
d
DO11.10+ Tfh cells (x10^6)
nsP=0.15123
**P=0.00124
***P=0.00087
GC B cells (x10^6)
nsP=0.3777
**P=0.0022
**P=0.0011
CD40L+ DO11.10+ T cells (x10^6)
nsP=0.44759
**P=0.00124
***P=0.00087
ICOS+ DO11.10+ T cells (x10^6)
nsP=0.44759
**P=0.00165
***P=0.00087

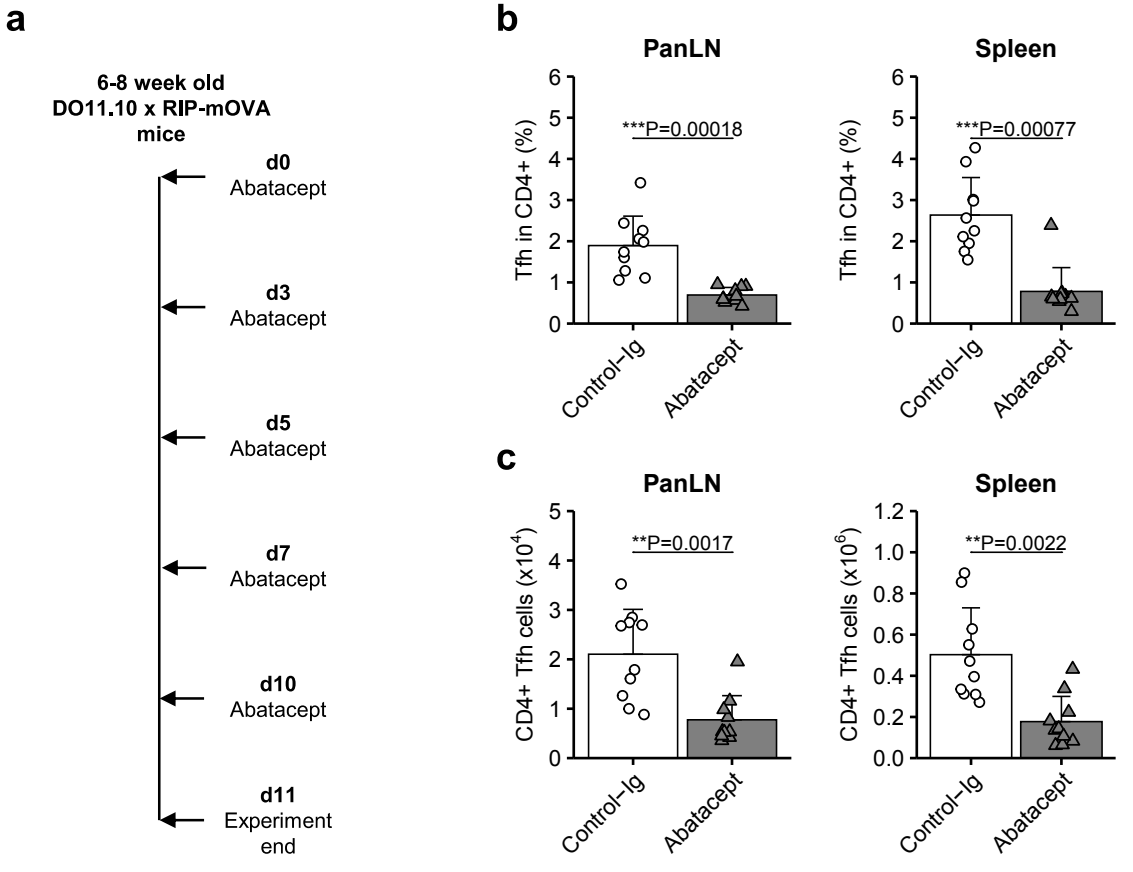
a
6-8 week old
DO11.10 x RIP-mOVA
mice
d0
Abatacept
d3
Abatacept
d5
Abatacept
d7
Abatacept
d10
Abatacept
d11
Experiment
end
b
PanLN
Spleen
Tfh in CD4+ (%)
***P=0.00018
***P=0.00077
Control-Ig
Abatacept
c
PanLN
Spleen
CD4+ Tfh cells (x10^4)
CD4+ Tfh cells (x10^6)
**P=0.0017
**P=0.0022
Control-Ig
Abatacept

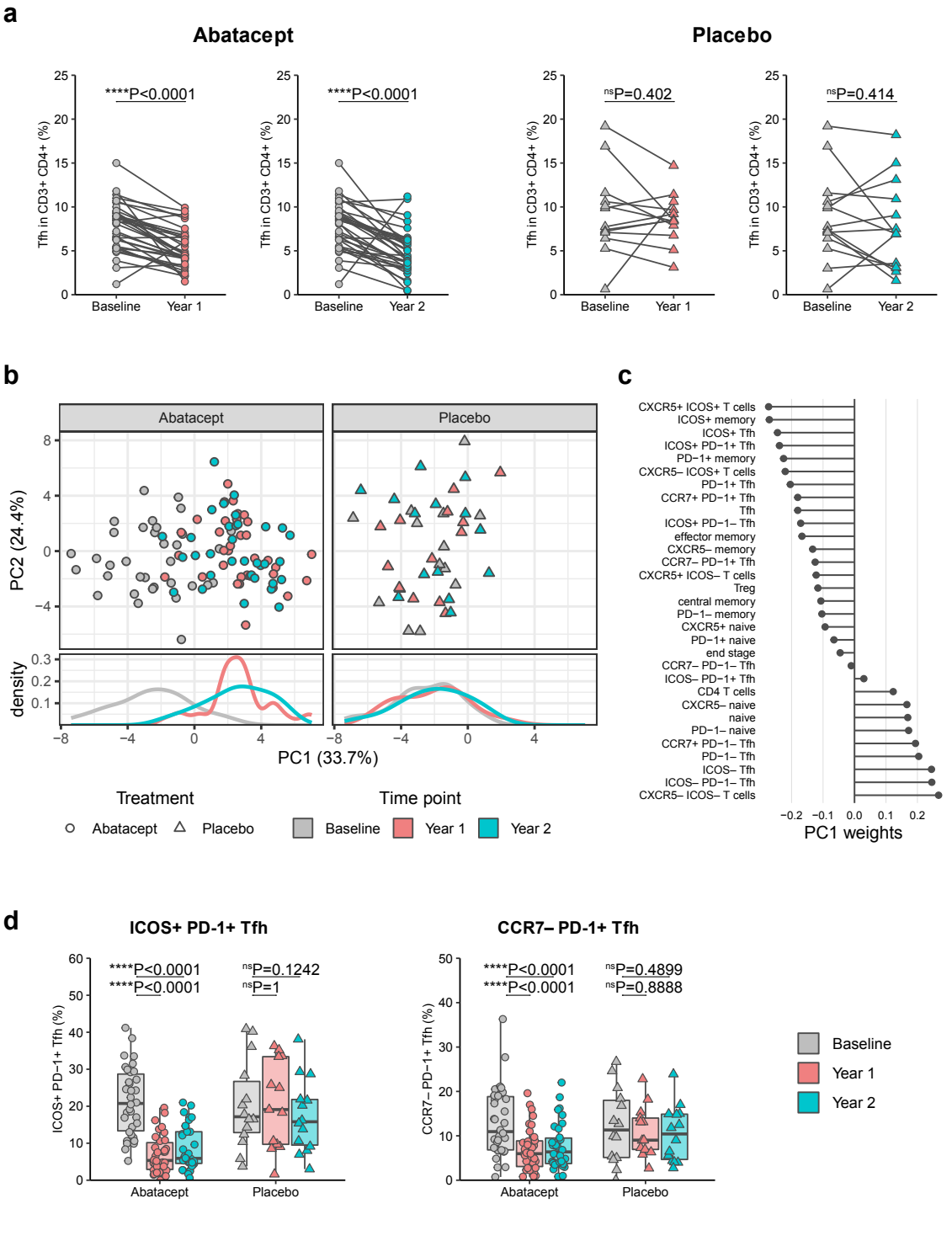
a
Abatacept
Placebo
Tfh in CD3+ CD4+ (%)
****P<0.0001
****P<0.0001
nsP=0.402
nsP=0.414
Baseline
Year 1
Year 2
b
Abatacept
Placebo
PC2 (24.4%)
density
PC1 (33.7%)
Treatment
Abatacept
Placebo
Time point
Baseline
Year 1
Year 2
c
CXCR5+ ICOS+ T cells
ICOS+ memory
ICOS+ Tfh
ICOS+ PD−1+ Tfh
PD−1+ memory
CXCR5− ICOS+ T cells
PD−1+ Tfh
CCR7+ PD−1+ Tfh
Tfh
ICOS+ PD−1− Tfh
effector memory
CXCR5− memory
CCR7− PD−1+ Tfh
CXCR5+ ICOS− T cells
Treg
central memory
PD−1− memory
CXCR5+ naive
PD−1+ naive
end stage
CCR7− PD−1− Tfh
ICOS− PD−1+ Tfh
CD4 T cells
CXCR5− naive
naive
PD−1− naive
CCR7+ PD−1− Tfh
PD−1− Tfh
ICOS− Tfh
ICOS− PD−1− Tfh
CXCR5− ICOS− T cells
PC1 weights
d
ICOS+ PD−1+ Tfh
****P<0.0001
****P<0.0001
nsP=0.1242
nsP=1
CCR7− PD−1+ Tfh
****P<0.0001
****P<0.0001
nsP=0.4899
nsP=0.8888
Abatacept
Placebo
Baseline
Year 1
Year 2

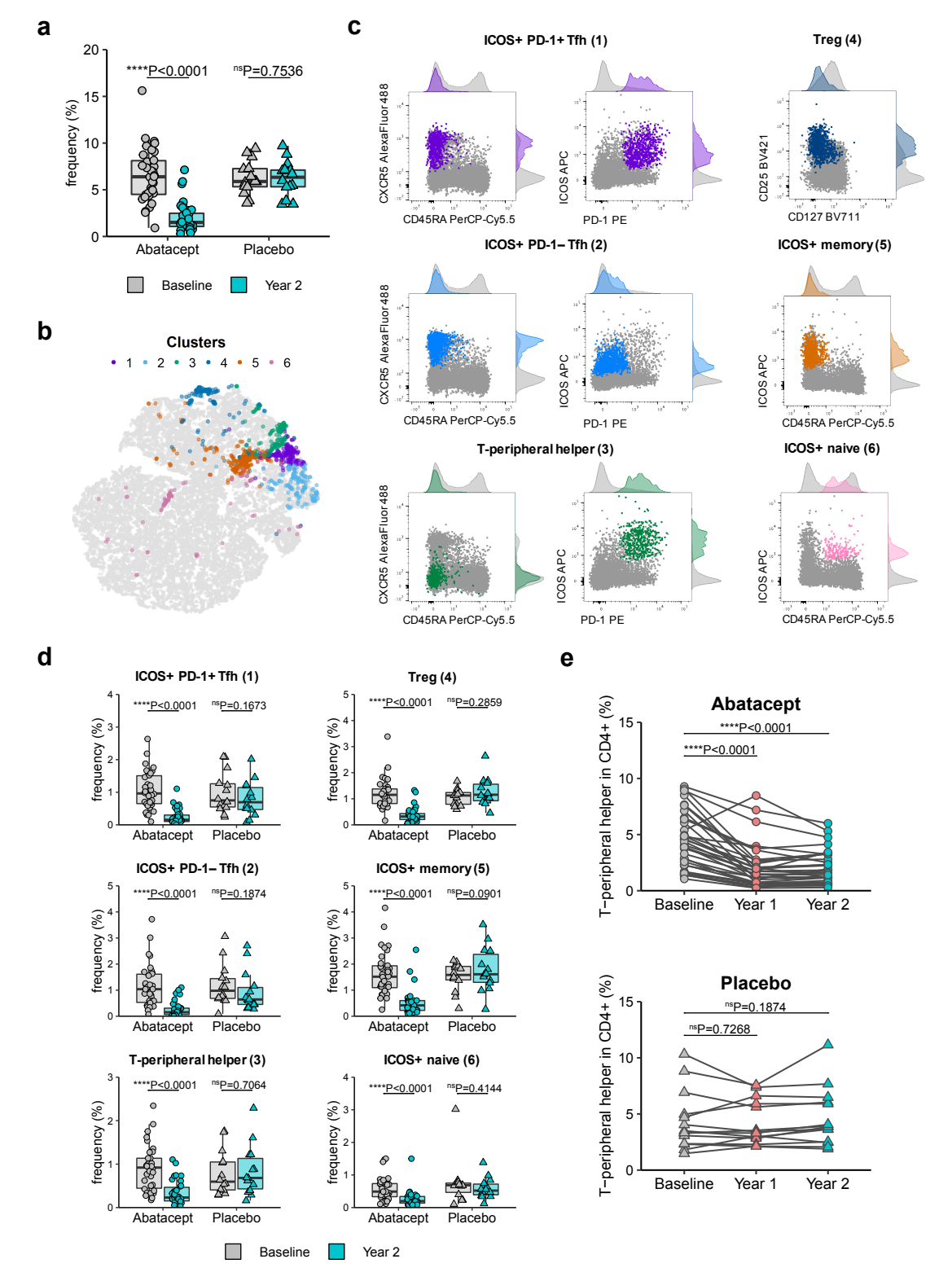
a
frequency (%)
****P<0.0001
nsP=0.7536
Abatacept
Placebo
Baseline
Year 2
b
Clusters
1 2 3 4 5 6
c
ICOS+ PD-1+ Tfh (1)
Treg (4)
ICOS+ PD-1– Tfh (2)
ICOS+ memory (5)
T-peripheral helper (3)
ICOS+ naive (6)
CXCR5 AlexaFluor 488
CD45RA PerCP-Cy5.5
ICOS APC
PD-1 PE
CD25 BV421
CD127 BV711
d
ICOS+ PD-1+ Tfh (1)
****P<0.0001
nsP=0.1673
Treg (4)
nsP=0.2859
ICOS+ PD-1– Tfh (2)
nsP=0.1874
ICOS+ memory (5)
nsP=0.0901
T-peripheral helper (3)
nsP=0.7064
ICOS+ naive (6)
nsP=0.4144
e
Abatacept
****P<0.0001
****P<0.0001
Placebo
nsP=0.1874
nsP=0.7268
T−peripheral helper in CD4+ (%)
Baseline
Year 1
Year 2

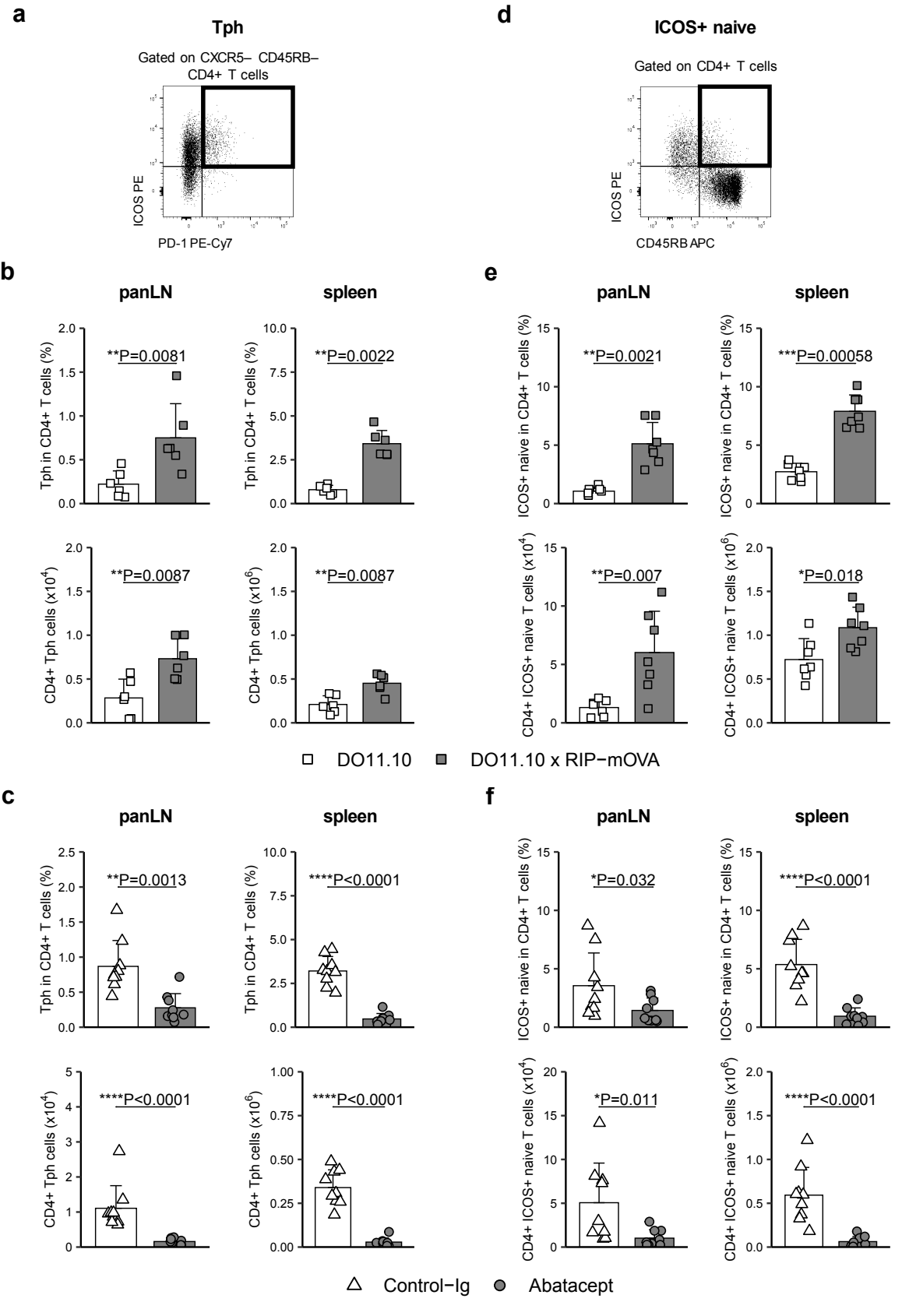
a
Tph
Gated on CXCR5– CD45RB–
CD4+ T cells
ICOS PE
PD-1 PE-Cy7
d
ICOS+ naive
Gated on CD4+ T cells
ICOS PE
CD45RB APC
b
panLN
spleen
Tph in CD4+ T cells (%)
**P=0.0081
**P=0.0022
CD4+ Tph cells (x10^4)
CD4+ Tph cells (x10^6)
**P=0.0087
**P=0.0087
e
panLN
spleen
ICOS+ naive in CD4+ T cells (%)
**P=0.0021
***P=0.00058
CD4+ ICOS+ naive T cells (x10^4)
CD4+ ICOS+ naive T cells (x10^6)
**P=0.007
*P=0.018
DO11.10
DO11.10 x RIP−mOVA
c
panLN
spleen
Tph in CD4+ T cells (%)
**P=0.0013
****P<0.0001
CD4+ Tph cells (x10^4)
CD4+ Tph cells (x10^6)
****P<0.0001
****P<0.0001
f
panLN
spleen
ICOS+ naive in CD4+ T cells (%)
*P=0.032
****P<0.0001
CD4+ ICOS+ naive T cells (x10^4)
CD4+ ICOS+ naive T cells (x10^6)
*P=0.011
****P<0.0001
Control−Ig
Abatacept

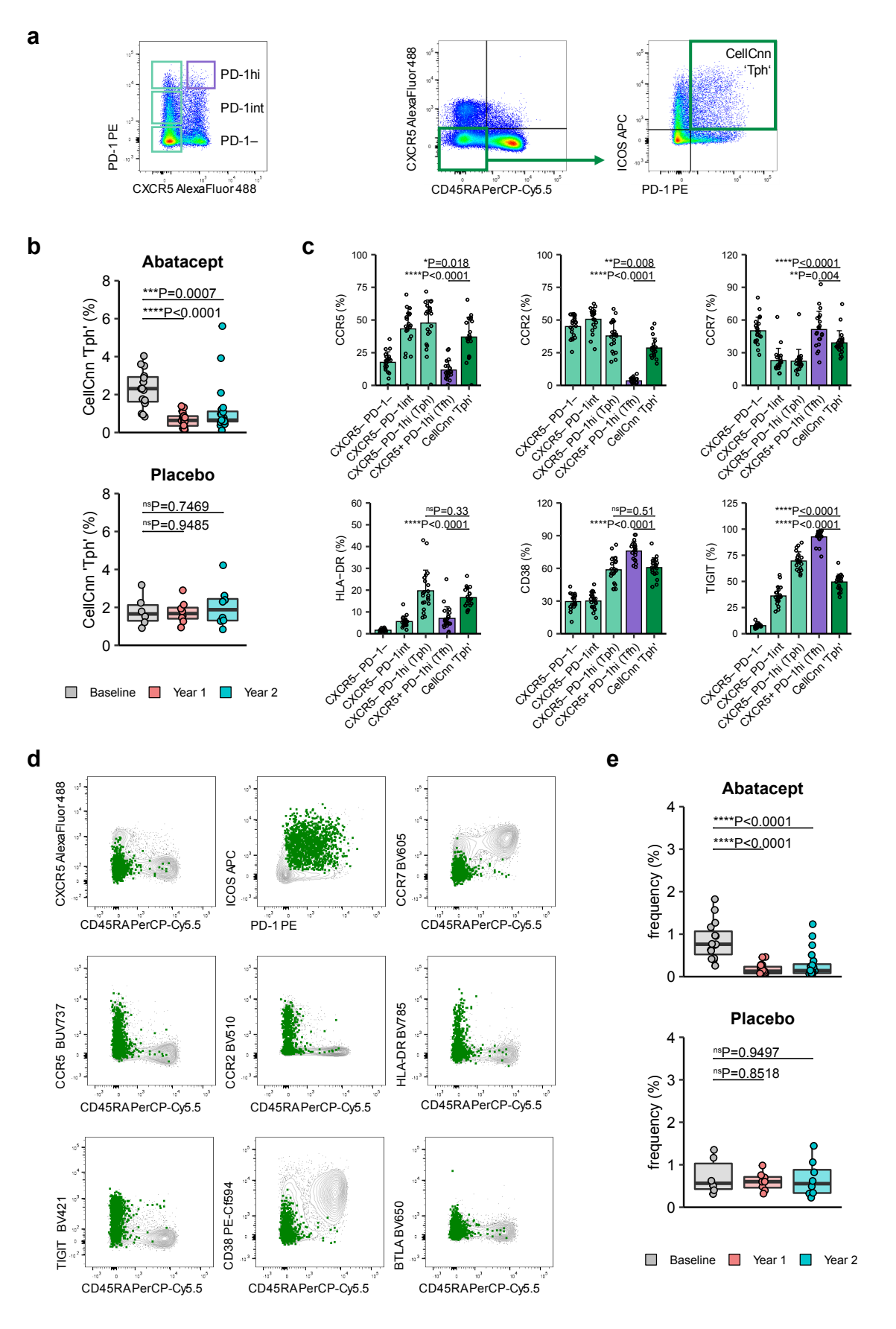
a
PD-1hi
PD-1int
PD-1–
PD-1 PE
CXCR5 AlexaFluor 488
CXCR5 AlexaFluor 488
CD45RAPerCP-Cy5.5
CellCnn 'Tph'
ICOS APC
PD-1 PE
b
Abatacept
***P=0.0007
****P<0.0001
CellCnn 'Tph' (%)
Placebo
nsP=0.7469
nsP=0.9485
CellCnn 'Tph' (%)
Baseline
Year 1
Year 2
c
*P=0.018
****P<0.0001
CCR5 (%)
**P=0.008
****P<0.0001
CCR2 (%)
****P<0.0001
**P=0.004
CCR7 (%)
nsP=0.33
****P<0.0001
HLA-DR (%)
nsP=0.51
****P<0.0001
CD38 (%)
****P<0.0001
****P<0.0001
TIGIT (%)
CXCR5– PD-1–
CXCR5– PD-1int
CXCR5– PD-1hi (Tph)
CXCR5+ PD-1hi (Tfh)
CellCnn 'Tph'
d
CXCR5 AlexaFluor 488
CD45RAPerCP-Cy5.5
ICOS APC
PD-1 PE
CCR7 BV605
CCR5 BUV737
CCR2 BV510
HLA-DR BV785
TIGIT BV421
CD38 PE-Cf594
BTLA BV650
e
Abatacept
****P<0.0001
****P<0.0001
frequency (%)
Placebo
nsP=0.9497
nsP=0.8518
frequency (%)
Baseline
Year 1
Year 2

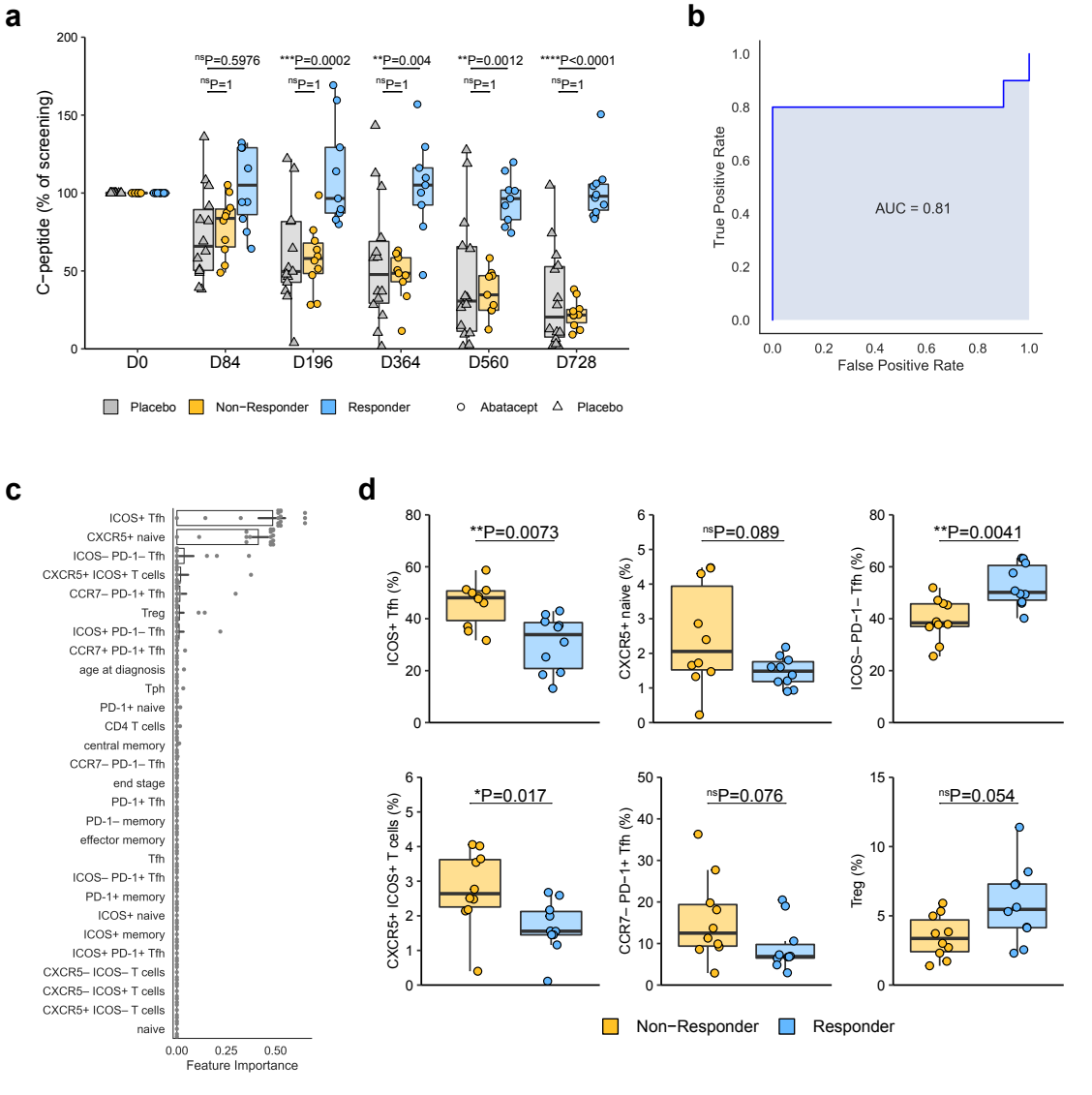
a
C−peptide (% of screening)
200
150
100
50
0
nsP=0.5976
nsP=1
***P=0.0002
nsP=1
**P=0.004
nsP=1
**P=0.0012
nsP=1
****P<0.0001
nsP=1
D0
D84
D196
D364
D560
D728
Placebo
Non−Responder
Responder
Abatacept
Placebo
b
True Positive Rate
False Positive Rate
AUC = 0.81
c
ICOS+ Tfh
CXCR5+ naive
ICOS− PD-1− Tfh
CXCR5+ ICOS+ T cells
CCR7− PD-1+ Tfh
Treg
ICOS+ PD-1− Tfh
CCR7+ PD-1+ Tfh
age at diagnosis
Tph
PD-1+ naive
CD4 T cells
central memory
CCR7− PD-1− Tfh
end stage
PD-1+ Tfh
PD-1− memory
effector memory
Tfh
ICOS− PD-1+ Tfh
PD-1+ memory
ICOS+ naive
ICOS+ memory
ICOS+ PD-1+ Tfh
CXCR5− ICOS− T cells
CXCR5− ICOS+ T cells
CXCR5+ ICOS− T cells
naive
0.00
0.25
0.50
Feature Importance
d
ICOS+ Tfh (%)
**P=0.0073
CXCR5+ naive (%)
nsP=0.089
ICOS− PD−1− Tfh (%)
**P=0.0041
CXCR5+ ICOS+ T cells (%)
*P=0.017
CCR7− PD−1+ Tfh (%)
nsP=0.076
Treg (%)
nsP=0.054
Non−Responder
Responder

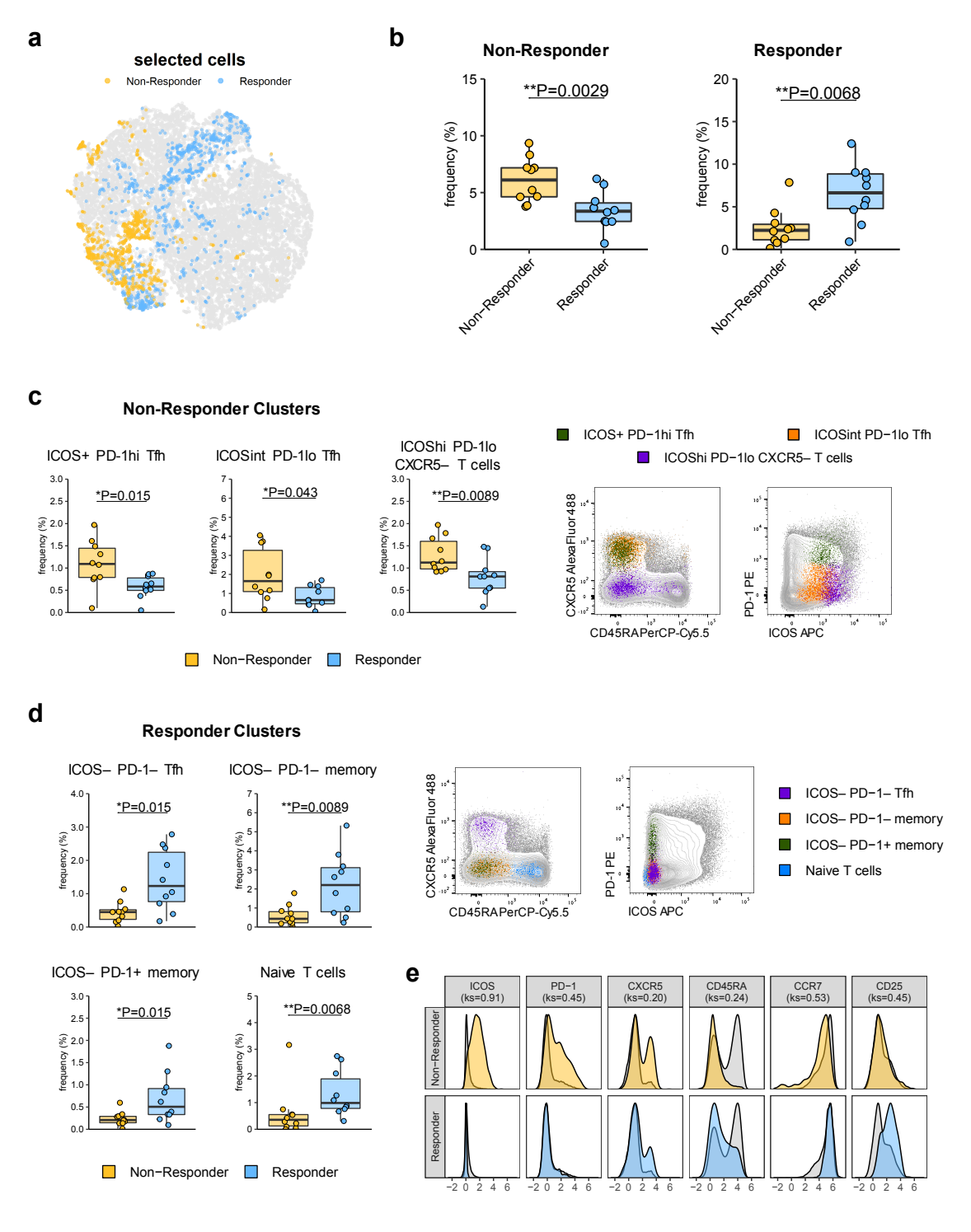
a
selected cells
Non-Responder
Responder
b
Non-Responder
Responder
**P=0.0029
**P=0.0068
frequency (%)
Non-Responder
Responder
c
Non-Responder Clusters
ICOS+ PD-1hi Tfh
ICOSint PD-1lo Tfh
ICOShi PD-1lo CXCR5– T cells
*P=0.015
*P=0.043
**P=0.0089
frequency (%)
ICOS+ PD-1hi Tfh
ICOSint PD-1lo Tfh
ICOShi PD-1lo CXCR5– T cells
CXCR5 AlexaFluor488
CD45RAPerCP-Cy5.5
PD-1 PE
ICOS APC
Non-Responder
Responder
d
Responder Clusters
ICOS– PD-1– Tfh
ICOS– PD-1– memory
ICOS– PD-1+ memory
Naive T cells
*P=0.015
**P=0.0089
*P=0.015
**P=0.0068
frequency (%)
CXCR5 AlexaFluor488
CD45RAPerCP-Cy5.5
PD-1 PE
ICOS APC
ICOS– PD-1– Tfh
ICOS– PD-1– memory
ICOS– PD-1+ memory
Naive T cells
Non-Responder
Responder
e
ICOS (ks=0.91)
PD-1 (ks=0.45)
CXCR5 (ks=0.20)
CD45RA (ks=0.24)
CCR7 (ks=0.53)
CD25 (ks=0.45)
Non-Responder
Responder
−2 0 2 4 6

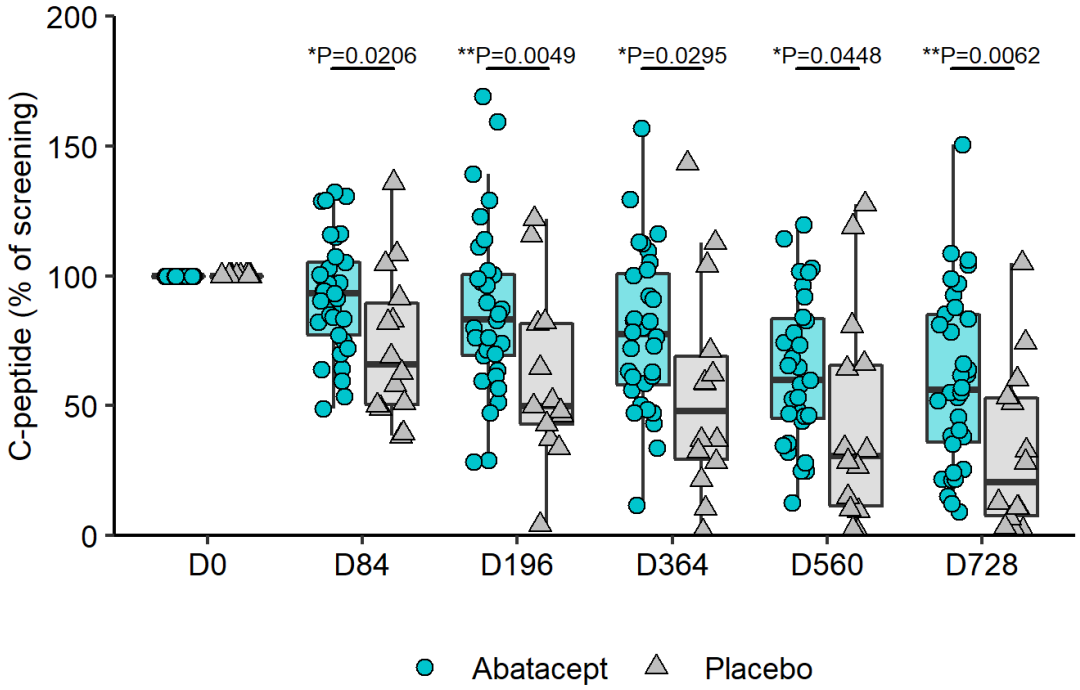

Supplementary Figure 1. Preserved C-peptide response in patients receiving Abatacept

C-peptide AUC per time point and treatment as % of screening C-peptide AUC for all patients. Shown are boxplots with black horizontal line denoting median value, while box represents IQR (Q1-Q3 percentile) and whiskers show minimum (Q1– 1.5 * IQR) and maximum (Q3 + 1.5 * IQR) values. Abatacept, n=31 (D560), 32 (D364), 33 (D84, D196) or 34 (D0, D728) patients; Placebo, n=13 (D196) or 14 (all other time points) patients. Two-tailed Mann–Whitney U test; **, $p < 0.01$; *, $p < 0.05$.

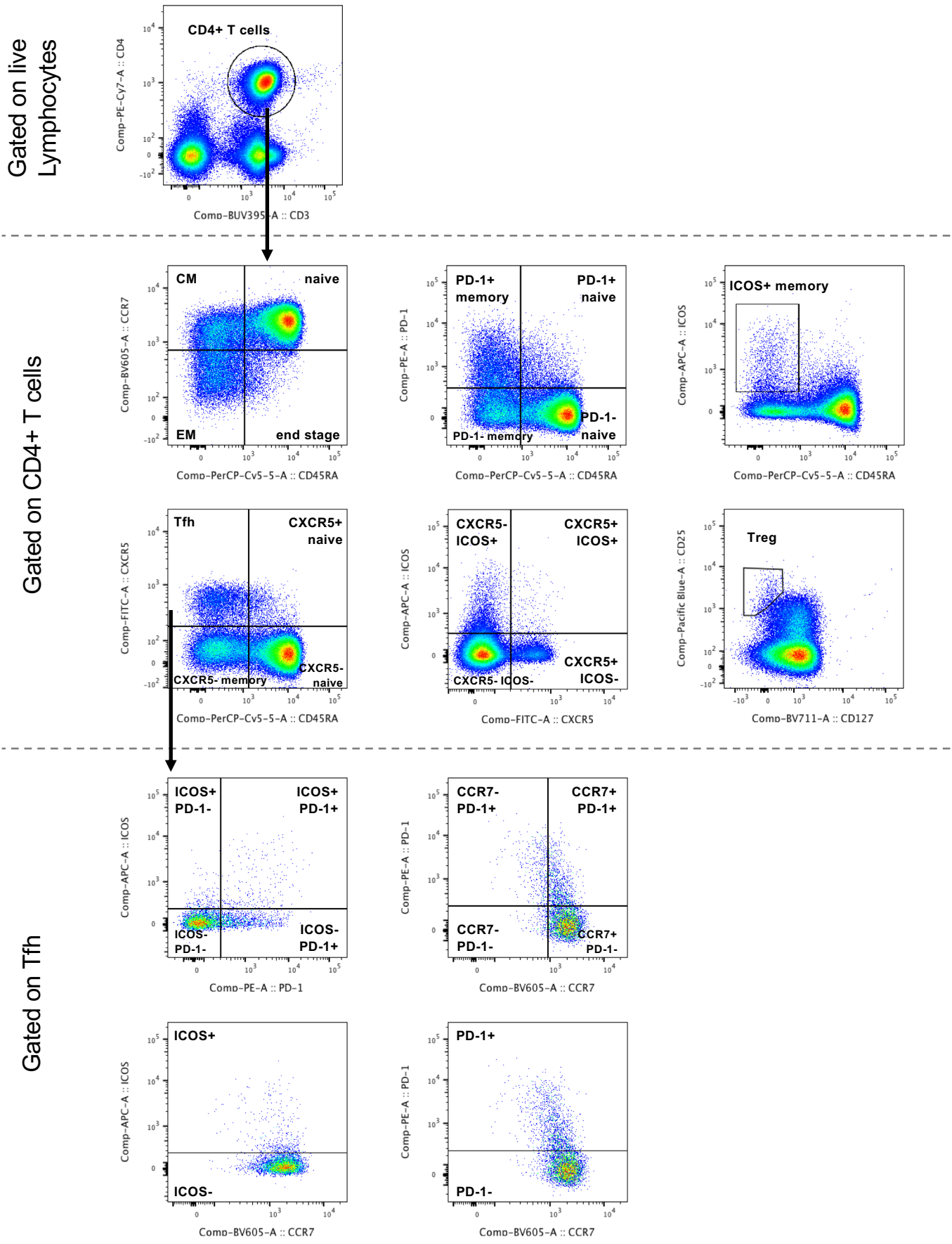

Supplementary Figure 2. Gating strategy

Representative gating strategy for patient samples stained for flow cytometry. PBMC samples were thawed and stained as described in the methods. Following an initial singlet gate and a live cell gate (not shown), populations were gated as presented. Names indicated are those used in downstream analysis. CM: central memory; EM: effector memory.

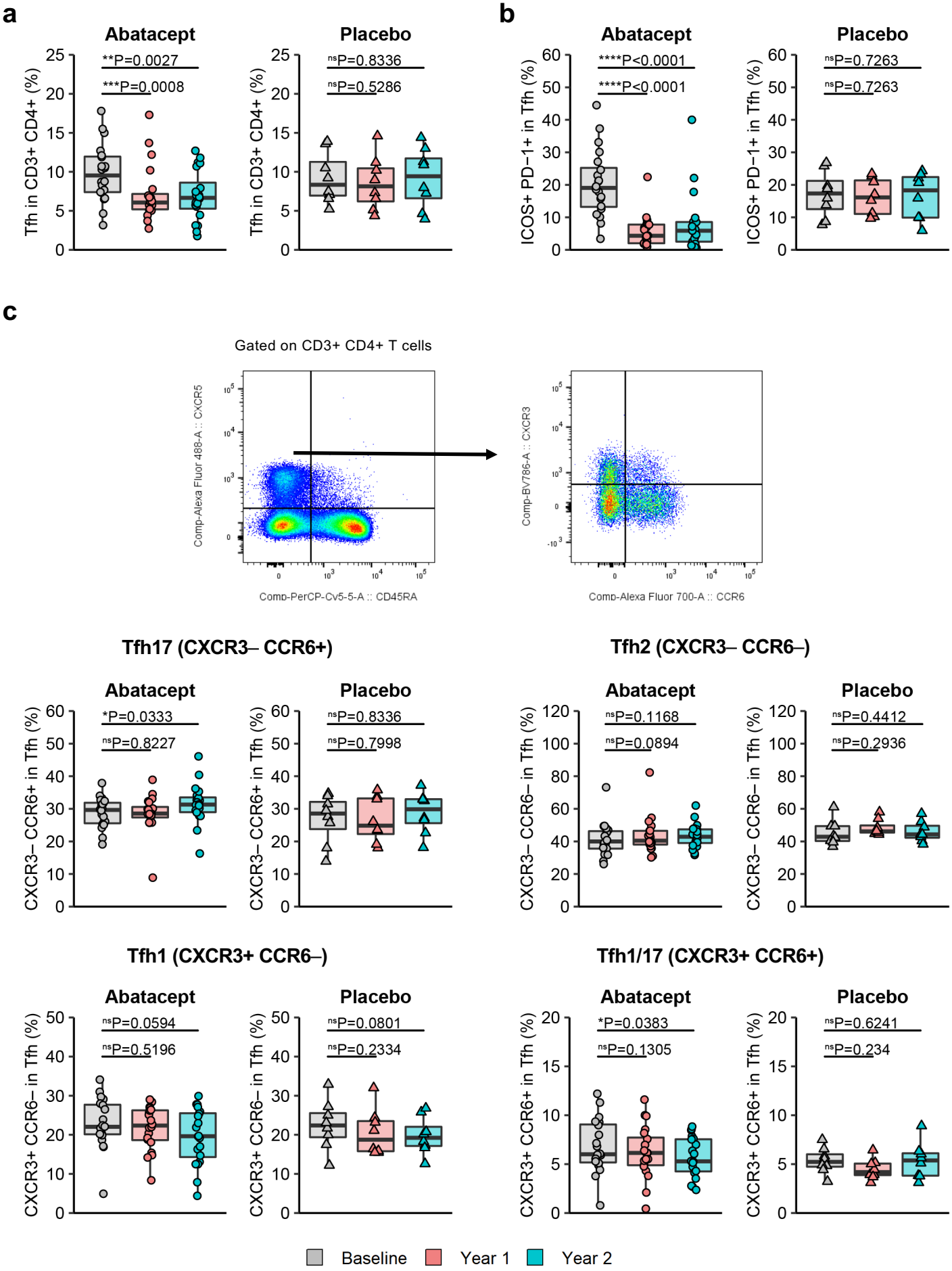

Supplementary Figure 3. Minimal impact of Abatacept treatment on Tfh skewing
See following page for full legend.

Supplementary Figure 3. Minimal impact of Abatacept treatment on Tfh skewing
Additional frozen PBMC samples from recent onset T1D patients that received Abatacept or placebo were thawed and stained for flow cytometry analysis of Tfh skewing. **(a)** Collated data for Tfh ($CD45RA^-$ $CXCR5^+$) frequencies in $CD3^+$ $CD4^+$ cells from recipients of Abatacept (left) or placebo (right) in new cohort. **(b)** Collated data for $ICOS^+$ $PD\text{-}1^+$ frequencies in Tfh cells from recipients of Abatacept or placebo in new cohort. **(c)** Representative gating strategy (top) and collated data (bottom) for frequencies of indicated populations of CXCR3 and CCR6 expressing Tfh cells in Abatacept and placebo treated individuals. Shown are boxplots with black horizontal line denoting median value, while box represents IQR (Q1-Q3 percentile) and whiskers show minimum (Q1– 1.5 * IQR) and maximum (Q3 + 1.5 * IQR) values. Abatacept, n=20 patients; Placebo, n=8 patients. Two-tailed Wilcoxon signed-rank test; ****, $p < 0.0001$; ***, $p < 0.001$; **, $p < 0.01$; *, $p < 0.05$; ns, not significant.

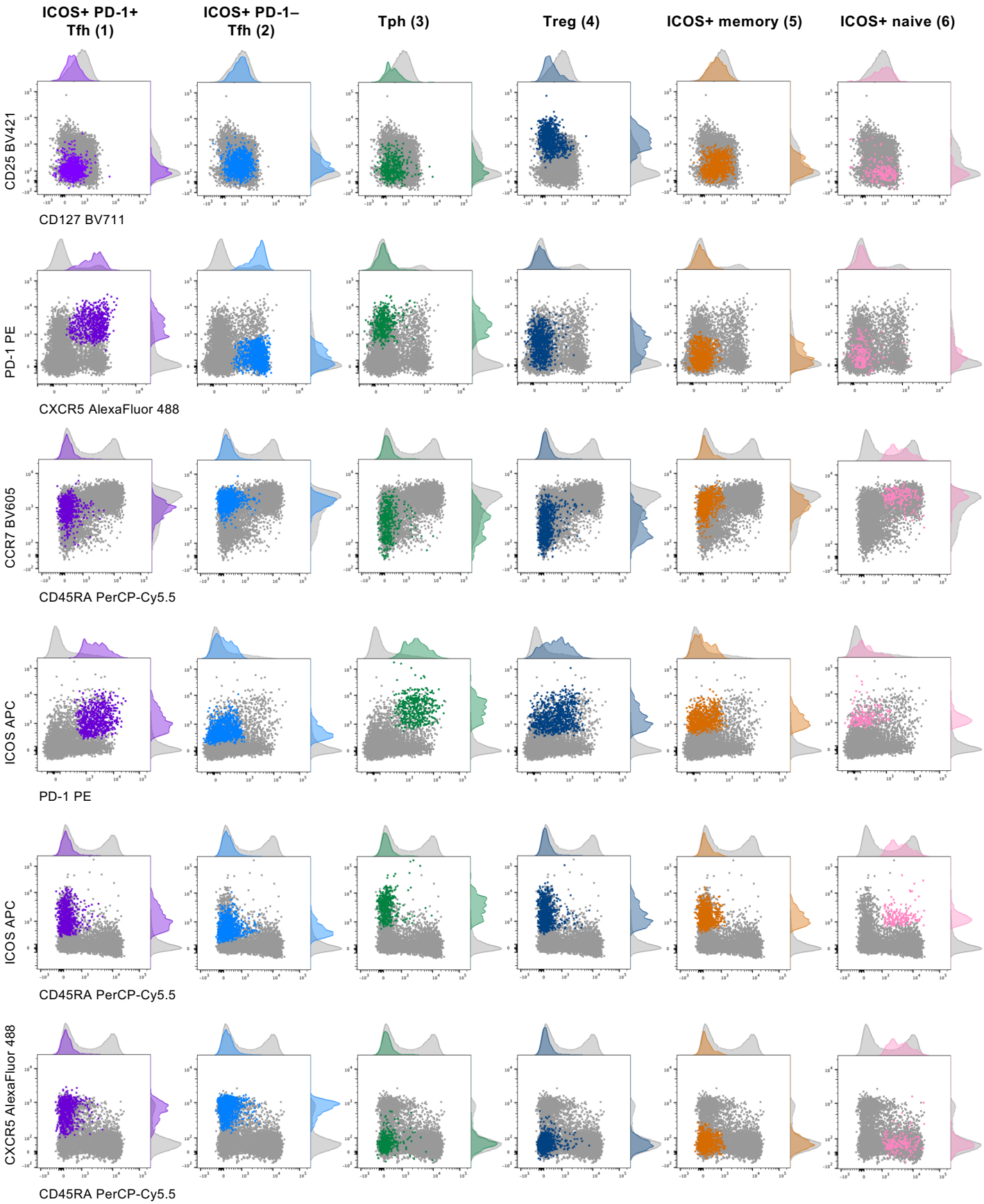

Supplementary Figure 4. Cell clusters identified by data-driven analysis correspond to known cell subsets

Cell clusters identified by CellCnn and k-means clustering to be significantly reduced in samples from Abatacept-treated individuals were overlaid onto flow cytometry data in order to infer identity. Plots show representative overlays of k-means clusters (colour) on original flow cytometry data (grey). Examples shown derive from a baseline sample.

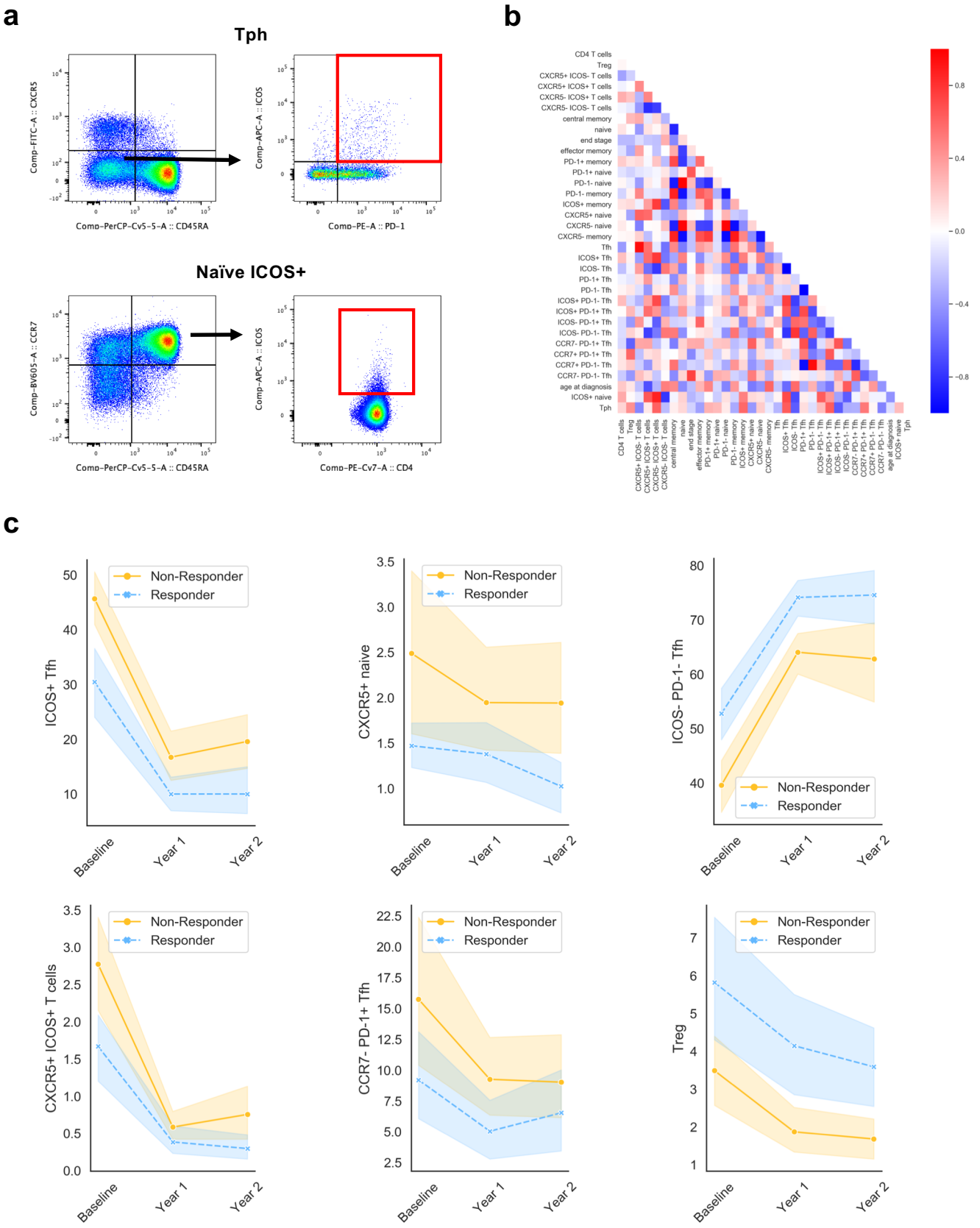

Supplementary Figure 5. Feature selection for gradient boosting model and dynamic analysis of cell populations

(a) Representative flow cytometry plots depicting manual gating strategy for the additional populations added prior to development of a predictive model. These two populations, Tph (top) and naive ICOS⁺ T cells (bottom), were added since they were identified by CellCnn and k-means clustering to be altered in Abatacept-treated individuals. **(b)** Pairwise Pearson correlation comparison of all features used in gradient boosting model. A threshold of 0.95 was used to eliminate highly correlated features. **(c)** Time-series plots of flow cytometry gated populations contributing to gradient boosting model. Mean and 95% confidence interval are plotted (n=10 patients in each group).

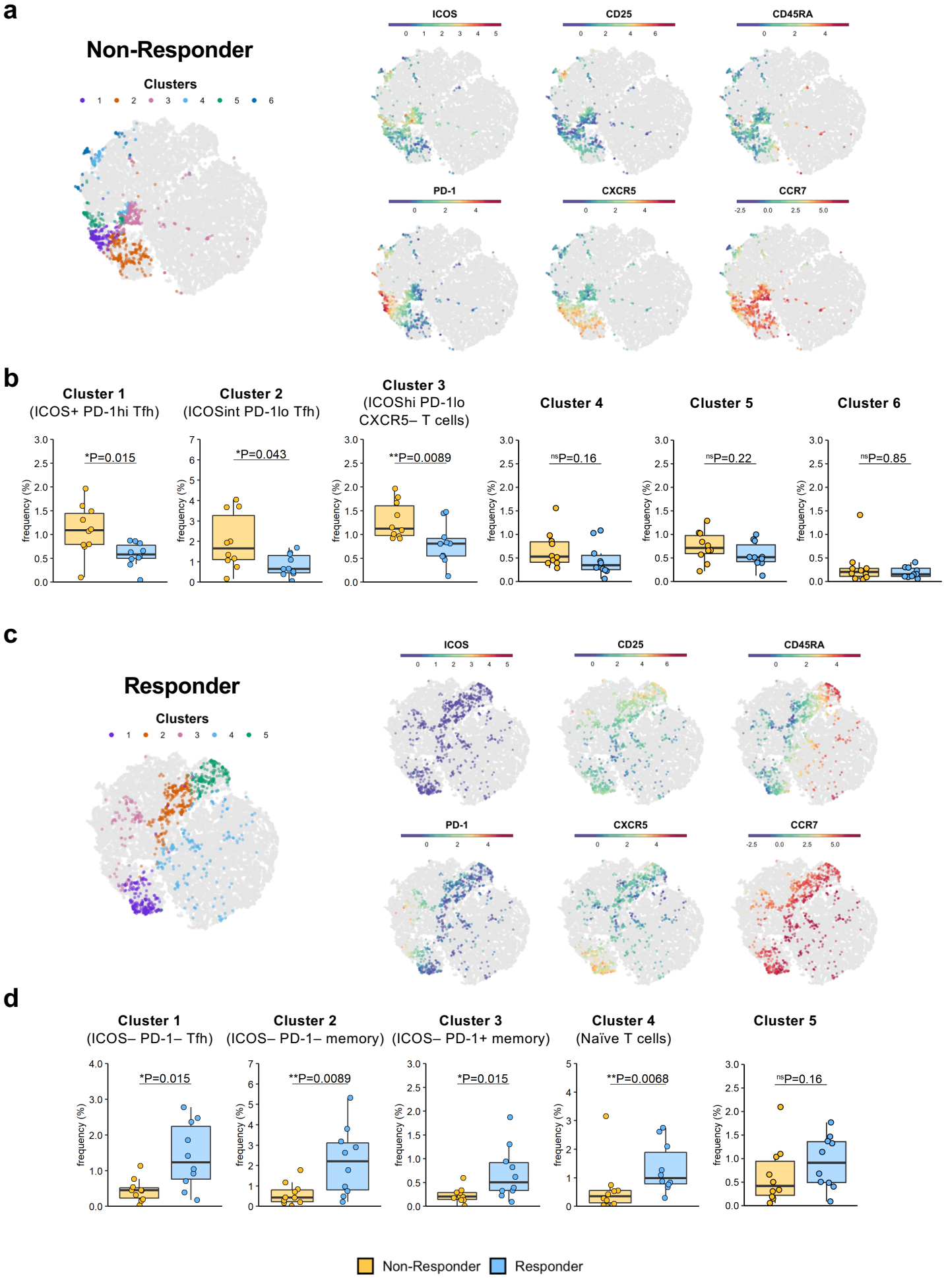

Supplementary Figure 6. Visualisation and frequencies of clusters identified by CellCnn that are linked to clinical response to Abatacept

See following page for full legend.

Supplementary Figure 6. Visualisation and frequencies of clusters identified by CellCnn that are linked to clinical response to Abatacept

Clustering results of CellCnn Responder vs Non-Responder comparison. t-SNE plot of marker expression and cluster assignment on selected cells (Responder vs Non-Responder comparison). **(a, c)** t-SNE projection of down-sampled, pooled flow cytometry data of all samples used for CellCnn analysis. K-means clusters or indicated marker expression of non-responder **(a)** and responder **(c)** filter-specific cells are highlighted. **(b, d)** Frequency of cluster-specific cells in each analysed sample for non-responder **(b)** and responder **(d)** filters. Shown are boxplots with black horizontal line denoting median value, while box represents IQR (Q1-Q3 percentile) and whiskers show minimum (Q1– 1.5 * IQR) and maximum (Q3 + 1.5 * IQR) values. n=10 patients in each group; two-tailed Mann-Whitney U test; **, $p < 0.01$; *, $p < 0.05$; ns, not significant.

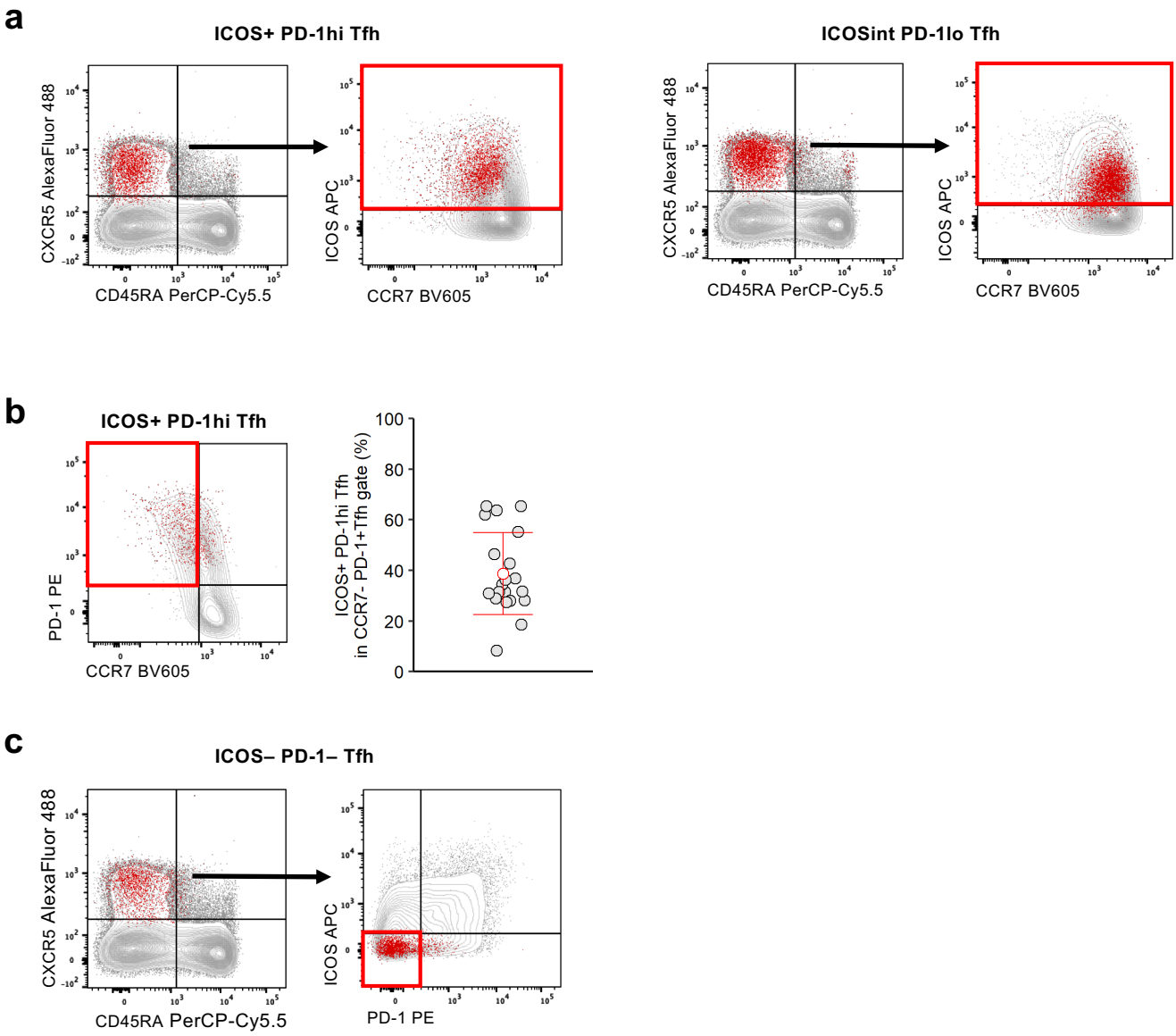

Supplementary Figure 7. Cell clusters identified by data-driven analysis overlay manually gated cell populations

CellCnn and k-means clustering were used to identify populations that differed between individuals showing a good or poor response to Abatacept. Identified populations were then overlaid onto manually gated flow cytometry plots. **(a)** Representative overlays of cells belonging to ICOS^{+} PD-1^{hi} Tfh (left) and ICOS^{int}PD-1^{lo} Tfh (right) CellCnn clusters (red) on manual gating for ICOS^{+} Tfh cells (grey). **(b)** Representative overlay of ICOS^{+} PD-1^{hi} Tfh CellCnn cluster (red) on CCR7^{-}PD-1^{+} Tfh gate (grey) (left). Collated data showing frequency of CellCnn cluster ICOS^{+} PD-1^{hi} Tfh that falls within manual CCR7^{-}PD-1^{+} Tfh gate (right). n=20 patients. Mean ± SD are plotted in red. **(c)** Representative overlay of cells belonging to ICOS^{-}PD-1^{-} Tfh CellCnn cluster (red) on manual gating for ICOS^{-} PD-1^{-} Tfh cells (grey). Examples shown are from a baseline sample.

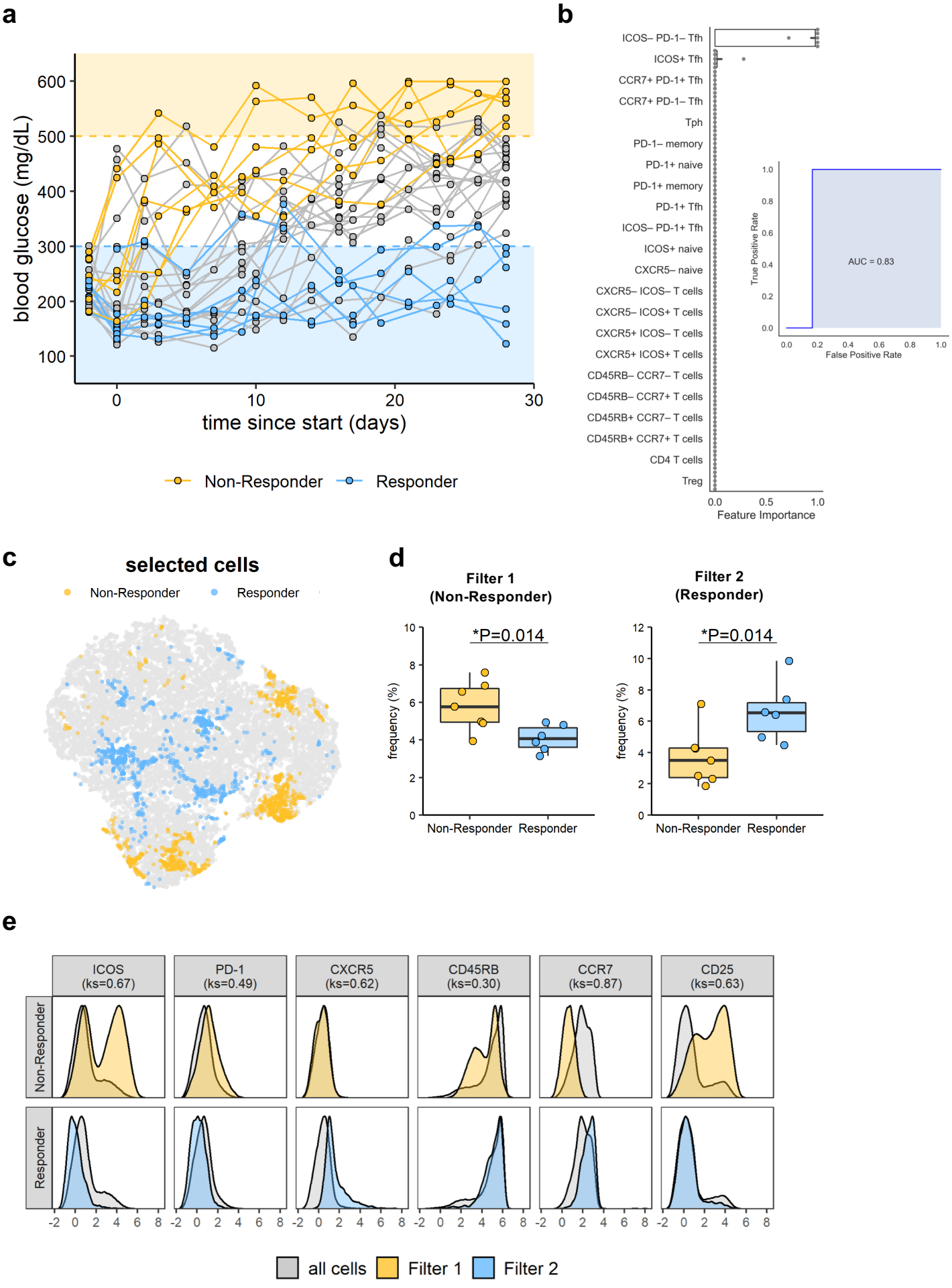

Supplementary Figure 8. Analysis of response to Abatacept in mouse model of autoimmune diabetes reveals similar trends to human data

See following page for full legend.

Supplementary Figure 8. Analysis of response to Abatacept in mouse model of autoimmune diabetes reveals similar trends to human data

Blood glucose of DO11.10 x RIP-mOVA mice was monitored and mice with blood glucose between 180 and 290 mg/dL were treated with Abatacept every two to three days for four weeks. Blood glucose was monitored, and responder and non-responder mice were identified based on final blood glucose reading. **(a)** Blood glucose readings of all treated mice over the treatment period. Responders and non-responders are highlighted in blue and yellow, respectively. Cut-offs used are highlighted in corresponding colour. **(b)** Baseline bleeds were stained for flow cytometry analysis and gated in a similar way to human samples, substituting CD45RB for CD45RA. The gradient boosting model used in Fig.7 was applied to this data after removal of highly correlated features. Features ranked by importance (bar shows mean and black lines represent 95% confidence intervals) and ROC curve of the predictive model are shown. **(c,d,e)** CellCnn analysis was applied to baseline samples of responders and non-responders. t-SNE projection of down-sampled, pooled flow cytometry data of all samples used for CellCnn analysis **(c)**, frequencies of filter-specific cells in each sample for Responder and Non-Responder filter **(d)** and histograms of marker expression of filter-specific cells (yellow; non-responder, blue; responder) or all cells (grey) **(e)** are shown. In **(d)** boxplots are shown with black horizontal line denoting median value, while box represents IQR (Q1-Q3 percentile) and whiskers show minimum (Q1– 1.5 * IQR) and maximum (Q3 + 1.5 * IQR) values. **(a)** n=31 mice; **(b-e)** n=6 (responder) or 7 (non-responder) mice; **(d)** two-tailed Mann–Whitney U test; **(e)** two-tailed Kolmogorov-Smirnov (ks) test; *, $p < 0.05$.